Scheduling and Power Allocation in a Cognitive Radar Network for Multiple-Target Tracking

Phani Chavali, *Student Member, IEEE*, and Arye Nehorai, *Fellow, IEEE*

Abstract—We propose a cognitive radar network (CRN) system for the joint estimation of the target state comprising the positions and velocities of multiple targets, and the channel state comprising the propagation conditions of an urban transmission channel. We develop a measurement model for the received signal by considering a finite-dimensional representation of the time-varying system function which characterizes the urban transmission channel. We employ sequential Bayesian filtering at the receiver to estimate the target and the channel state. We propose a hybrid Bayesian filter that operates by partitioning the state space into smaller subspaces and thereby reducing the complexity involved with high-dimensional state space. The feedback loop that embodies the radar environment and the receiver enables the transmitter to employ approximate greedy programming to find a suitable subset of antennas to be employed in each tracking interval, as well as the power transmitted by these antennas. We compute the posterior Cramér–Rao bound (PCRB) on the estimates of the target state and the channel state and use it as an optimization criterion for the antenna selection and power allocation algorithms. We use several numerical examples to demonstrate the performance of the proposed system.

Index Terms—Adaptive power allocation, adaptive scheduling, Bayesian inference, cognitive radar network, complex urban environment, multi-target tracking, sequential Monte Carlo estimation.

I. INTRODUCTION

THE term "cognitive radar" was first coined by the authors of [1] in 2006. The motivation for this idea comes from the echo location system of a bat. A bat uses its brain to perceive the environment, and then makes decisions based on the information it gains through the perception. The two separate activities, perception and decision, act together in a coordinated fashion, in a perception–action cycle, which forms the heart of the bat's echo location system. The authors of [1] propose an analogous cognitive system which is capable of perceiving the environment and adjusting its control, through feedback, to improve the overall system performance. With this motivation, three essential features have been identified which constitute the operation of a cognitive radar: Bayesian inference at the receiver, which enables information preservation; feedback from the receiver to the transmitter, which facilitates intelligent control; and adaptive processing at the transmitter, which builds on learning through the interaction of the radar with the environment. Nevertheless, the fundamental difference between the echo-location of a bat and a surveillance radar system is that a bat focusses on a single target at a time, but the radar system has to deal with multiple targets. This difference makes the cognitive information processing much more challenging and computationally intensive.

A cognitive radar network [2] incorporates several radars working together to achieve the task of enhanced remote sensing capability. The network can operate in two modes, distributed cognition and central cognition. In a distributed cognitive network, each radar is capable of cognitive processing, whereas in a central cognitive network, a single radar acts as the brain of the entire network. With several radars operating in parallel, the system performance is considerably improved over a single radar. Several problems have been addressed in the past under the closed-loop cognitive framework. The authors of [3] integrate waveform design, based on the maximization of mutual information, with sequential hypothesis testing, and in [4], mutual information was used as an optimization criterion to improve the target detection probability and the delay-Doppler resolution. In [5], the authors use a cognitive radar for single-target tracking and propose a waveform optimization based on the minimization of the posterior Cramér–Rao bound (PCRB). In [6], the authors employ dynamic programming to select optimal waveforms from a prescribed library using PCRB as an optimization criterion. In [7], the authors use a cognitive radar network for extended target recognition, and in [8], the authors propose an adaptive waveform design for a cognitive radar designed for target recognition. Finally, in [9], the authors describe time resource allocation techniques for a cognitive radar system.

In this paper, we use a cognitive radar network for the task of tracking multiple-targets [10]. The problem of multiple-target tracking has been of great interest for various commercial and military applications. When the targets are moving in a dense urban environment, this problem becomes much more challenging [11]–[13]. The propagation path in such an environment consists of multiple scatterers, which can be in relative motion with respect to the sensors. This introduces both delay and Doppler shift in the received signals. To exploit this inherent delay-Doppler diversity and to obtain better performance, accurate priori information about the multipath channel state is required. When no prior information is available, the channel state has to be estimated along with the target state.

When multiple sensors are employed, the channel state between each pair of sensors has to be estimated. Hence, the problem of tracking multiple targets in complex scenarios, such as an urban environment, poses a computational challenge due to the high-dimensionality of the state space.

The major contributions of this work are threefold. First, we extend the sequential Bayesian inference framework proposed in [14] to the case of a cognitive radar network operating in an urban scenario, characterized by delay and Doppler spread, for the joint estimation of the target state and the channel state. The exact solution to the estimation problem cannot be found, since the sensing model is nonlinear. Hence, we employ a particle filter, which uses sequential Monte Carlo methods, for obtaining an approximate Bayesian estimate of the state vector. However, estimation using the standard particle filter (SPF) requires large number of particles to obtain an accurate estimate of the high-dimensional state vector. We propose a hybrid filter, which is a combination of a multiple particle filter (MPF) and a Rao–Blackwellized particle filter (RBPF), by exploiting the structure of the state space. Second, we derive the closed-form expressions for the PCRB on the estimates of the state vector, when the received signal at each radar is a linear combination of the delayed and Doppler-shifted versions of the signals transmitted from all the radars. Specifically, we do not assume that the signals transmitted by the individual radars are orthogonal to each other for all the delay and Doppler pairs. Third, we look at the problems of adaptive sensor scheduling and power allocation for the cognitive radar network. Since the total costs of acquiring measurements, the communication involved with central processing, and the computational complexity of processing the measurements, increases with the number of operational radars, it is important to adaptively select a subset of operational radars and the power allocated to them at each time, to minimize the error in the estimate of the state vector. The problem of selecting a subset of sensors from a given set of possible sensors arises in various applications and has been addressed in the literature for passive networks [15]. The estimation performance is evaluated using the volume of the confidence ellipsoid as a performance metric, which is minimized for finding a suitable subset of sensors to be employed. For an active sensor network, such as a radar network, it is also important to consider the constraints on the signal power to be transmitted, and the sensor locations while formulating the optimization problem. Few works in the past have addressed the problem of sensor scheduling for active sensor networks like a distributed MIMO radar network. In [16] and [17], the authors propose a subset selection algorithm for the task of estimating the position of a single stationary target. They do not assume the presence of multipath and assume that the signals transmitted from each radar to be orthogonal. In [18], authors consider tracking multiple targets, but they also do not consider multipath and assume that the transmitted signals are orthogonal. They perform an iterative local search to minimize the PCRB and find a subset of antennas to be employed at each time. In this paper, we consider tracking multiple targets moving in a multipath scenario. We derive the PCRB for arbitrary transmit signals and use that as an optimization criterion for the scheduling and power allocation problems. We propose a two-pass greedy algorithm for finding a suitable antenna

subset in the first pass and the power to be transmitted by the selected antennas in the second pass. Our algorithm is adaptive, and we select the antennas to be used and the power to be transmitted in each tracking interval based on the target state and the channel state estimates, which are obtained through the feedback from the receiver, with suitable constraints on the overall transmit power and communication cost. Hence, the adaptive scheduling and power allocation can be considered as a reaction of the cognitive transmitter to the environment perceived by the receiver, in order to minimize the overall error of the system.

The rest of the paper is organized as follows. We describe the system model in Section II, where we discuss the time-varying multipath characterization in an urban environment, measurement model, and the state space model. In Section III, we describe the proposed algorithm for the joint tracking of the target state and the channel state. In Section IV, we derive the PCRB on the state estimates and use it as an optimality criterion to solve the scheduling and power allocation problem. We provide several numerical results in Section V and draw conclusions in Section equation .

We use the following notations in the paper. We denote vectors by boldface lowercase letters, e.g., $\boldsymbol{a}$, and matrices by boldface uppercase letters, e.g., $\boldsymbol{A}$. For a matrix $\boldsymbol{A}$, we use $\boldsymbol{a}_i$ to represent the ith column of $\boldsymbol{A}$ and $[\boldsymbol{A}]_{ij}$ to represent the element in the ith row and the jth column. $(\boldsymbol{A})^T, (\boldsymbol{A})^H$, and $\text{vec}(\boldsymbol{A})$ denote the transpose, conjugate transpose and vector form of the matrix $\boldsymbol{A}$, respectively. The ith element of a vector $\boldsymbol{a}$ is denoted by a_i. The Kronecker product of two matrices, $\boldsymbol{A}$ and $\boldsymbol{B}$, is denoted as $\boldsymbol{A} \otimes \boldsymbol{B}$. $\boldsymbol{I}_M$ and $\boldsymbol{0}_{M \times N}$ denote an identity matrix of order M and a zero matrix of size $M \times N$, respectively. $*$ denotes the convolution operator, while $\Re\{x\}$ and $\Im\{x\}$ denote the real and imaginary parts of a complex number x.

II. System Model

We consider a network of P monostatic radars labeled as $\mathcal{P} = \{1, 2, \ldots, p, \ldots, P\}$ operating in a centralized fashion, i.e., information fusion, scheduling and resource allocation are confined to a central fusion center. The radar network is employed in the region of interest $\mathcal{R} \subset \mathbb{R}^2$, with the pth radar located at (x_p, y_p). One of the P radars will act as the fusion center for the network, and, without the loss of generality, we consider the first radar to be the fusion center of the network and that it is located at (0,0). There are M point targets moving in the region of interest $\mathcal{R}$, with the position and velocity of the mth target given as (x_m, y_m) and $(\dot{x}_m, \dot{y}_m)$. We abuse the notation slightly here and use the same symbols x and y to denote the x- and the y- positions of the radar and the target; we differentiate between them based on the subscript used for indexing the radar antennas and the targets. Throughout this paper, we use the subscript m to denote the target. All the other subscripts correspond to the radar antennas. Other than the targets, there are multiple scatters in the region $\mathcal{R}$, which can be stationary or moving at speeds comparable to the speed of the targets. The propagation path consists of a forward transmission channel, which is the path taken by the signal from the radar to the target, the target itself, and a reverse transmission channel, which is the path taken by the back scattered signal from the target to the radar (see Fig. 1). When there are no scatterers present, the forward transmission channel and
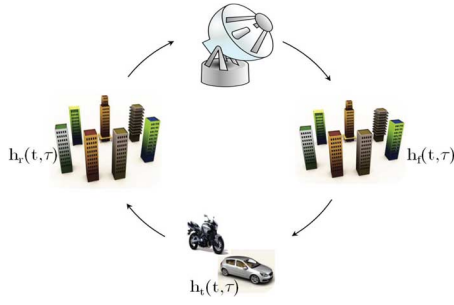
Fig. 1. Block diagram showing the forward transmission channel, the reverse transmission channel, and the targets.

the reverse transmission channel do not have any effect on the backscattered signal, except possibly a propagation loss. However, the presence of multiple scatterers in the environment introduces a delay spread in the forward and the reverse transmission channels, and the relative motion between the targets and the scatterers introduces time variations, which manifest as Doppler spread. We model the forward and the reverse transmission channels as linear time-varying systems and let $h_f(t, \tau)$ and $h_r(t, \tau)$ denote the response of the forward channel and the reverse channel, respectively. The overall channel response at delay τ and time t is then given as $h(t, \tau) = h_f(t, \tau) * h_r(t, \tau)$ [19].

A. Measurement Model

At each antenna, we transmit a coherent train of multiple pulses with a pulse repetition period of t_p seconds. The transmitted signal at the qth radar is given as

$$s_q(t) = \sum_{l=0}^{L-1} a_{lq}(t - lt_p) \tag{1}$$

where $a_{lq}(t)$ is the transmitted signal in the lth pulse from the qth radar. We use orthogonal-frequency-division multiplexing (OFDM) signaling [20] in each pulse with G subcarriers. The transmitted signal in l^{th} pulse is given as

$$a_{lq}(t) = \sum_{g=0}^{G-1} a_{lq}^g e^{j2\pi g \Delta f t} u(t),$$
$$l = 0, \ldots, L-1 \text{ and } q = 1, \ldots, P \tag{2}$$

where a_{lq}^g is the transmitted symbol in the gth subcarrier, l^{th} pulse and q^{th} antenna, $\boldsymbol{a}_{lq} = [a_{lq}^0, \ldots, a_{lq}^{G-1}]^T$, and $\Delta f = \frac{B}{G}$ is the subcarrier spacing. Let τ_{pqm} be the total time taken for the signal to travel from the qth radar to the mth target and back to the pth radar, and ν_{pqm} be the Doppler frequency shift due the qth, p^{th} transmit–receive pair and the mth target. The parameters τ_{pqm} and ν_{pqm} depend on the position and velocity of the mth target and the positions of the pth radar and the qth radar. We have

$$\tau_{pqm} = \frac{1}{c}\Big\{R_{qm} + R_{pm}\Big\} \tag{3}$$

and

$$\nu_{pqm} = \frac{f_c}{c}\Big\{\dot{R}_{qm} + \dot{R}_{pm}\Big\} \tag{4}$$

where c is the speed of propagation, f_c is the carrier frequency, R_{qm} is the range from the radar q to the target m, R_{pm} is the range from the radar p to the target m, and $\dot{R}_{qm}$ and $\dot{R}_{pm}$ are the corresponding range rates, i.e.,

$$R_{qm} = \sqrt{(x_q - x_m)^2 + (y_q - y_m)^2}$$
$$R_{pm} = \sqrt{(x_p - x_m)^2 + (y_p - y_m)^2}$$
$$\dot{R}_{qm} = \frac{\dot{x}_m(x_q - x_m) + \dot{y}_m(y_q - y_m)}{R_{qm}}$$

and

$$\dot{R}_{pm} = \frac{\dot{x}_m(x_p - x_m) + \dot{y}_m(y_p - y_m)}{R_{pm}}. \tag{5}$$

The received signal at the pth radar, due to the signal transmitted from the qth radar and bouncing off the mth target, is given as [19]

$$y_{pqm}(t) = \alpha_m \sqrt{\gamma_q \zeta_{pqm}} \int h_{pqm}(t, \tau) s_q$$
$$\times (t - \tau_{pqm} - \tau) e^{j2\pi\nu_{pqm}(t-\tau)} d\tau + w_p(t) \tag{6}$$

where
- α_m is the radar cross section (RCS) of the mth target;
- γ_q is the transmitted signal energy from the qth radar;
- $\zeta_{pqm} \propto \frac{1}{R_{qm}^2 R_{pm}^2}$ represents the path loss effects;
- $h_{pqm}(t, \tau)$ denotes the overall response of the channel between the qth radar, m^{th} target, and the pth radar, at delay τ and time t;
- $w_p(t)$ is the additive noise at the pth receiver.

The noise is assumed to be circularly symmetric, complex, white, and following a Gaussian distribution. If we consider the Fourier transform of $h_{pqm}(t, \tau)$, the signal $y_{pqm}(t)$ can be expressed as

$$y_{pqm}(t) = \alpha_m \sqrt{\gamma_q \zeta_{pqm}} \int \int H_{pqm}(f, \tau) s_q$$
$$\times (t - \tau_{pqm} - \tau) e^{j2\pi\nu_{pqm}(t-\tau)} e^{j2\pi ft} d\tau df + w_p(t). \tag{7}$$

A finite dimensional representation of (7) is obtained by sampling the delay-Doppler plane at the resolutions $\Delta\tau$ and Δf, such that $\tau \times f \in [0, T_d] \times [-\frac{B_d}{2}, \frac{B_d}{2}]$, where T_d and B_d represent the delay spread and the Doppler spread of the channel,[1] respectively. Equation (7) can then be expressed as

$$y_{pqm}(t) = \sqrt{\gamma_q \zeta_{pqm}} \sum_{n_f = -\frac{N_f}{2}}^{\frac{N_f}{2}-1} \sum_{n_\tau=0}^{N_\tau-1} \alpha_m H_{pqm}(n_f \Delta f, n_\tau \Delta\tau)$$
$$\times s_q(t - \tau_{pqm} - n_\tau \Delta\tau) e^{j2\pi\nu_{pqm}(t-n_\tau\Delta\tau)} e^{j2\pi n_f \Delta f t}$$
$$+ w_p(t)$$
$$= \sqrt{\gamma_q \zeta_{pqm}} \sum_{n_f = -\frac{N_f}{2}}^{\frac{N_f}{2}-1} \sum_{n_\tau=0}^{N_\tau-1} \beta_{pqm}^{n_f n_\tau} s_q(t - \tau_{pqm} - n_\tau \Delta\tau)$$
$$\times e^{j2\pi(\nu_{pqm} + n_f \Delta f)t} + w_p(t)$$

[1]The delay spread and the Doppler spread of the channel are the inverse of coherence bandwidth and the coherence time of the channel, respectively. Coherence time and coherence bandwidth denote the range of time scales and frequencies over which the variations caused due to the channel are constant

$$= \sqrt{\gamma_q \zeta_{pqm}} \sum_{n_f=-\frac{N_f}{2}}^{\frac{N_f}{2}-1} \sum_{n_\tau=0}^{N_\tau-1} \sum_{l=0}^{L-1} \beta_{pqm}^{n_f n_\tau}$$
$$\times a_{lq}(t - lt_p - \tau_{pqm} - n_\tau \Delta \tau) e^{j2\pi(\nu_{pqm}+n_f \Delta f)lt_p}$$
$$+ w_p(t) \qquad (8)$$

where $N_f = \lceil \frac{B_d}{\Delta f} \rceil$, $N_\tau = \lceil \frac{T_d}{\Delta \tau} \rceil$ and $\beta_{pqm}^{n_f n_\tau} = \alpha_m H_{pqm}(n_f \Delta f, n_\tau \Delta \tau)$. Since $a(t)$ is a narrow pulse, in arriving at (8), within each $a(t)$, we have approximated the term $e^{j2\pi\nu_{pqm}t}$ as $e^{j2\pi\nu_{pqm}lt_p}$ (a constant) and $e^{j2\pi n_f \Delta ft}$ as $e^{j2\pi n_f \Delta flt_p}$. The resolution of the sampling of the delay-Doppler plane is chosen to match the signaling duration and bandwidth, i.e., $\Delta \tau = \frac{1}{B}$ and $\Delta f = \frac{1}{T}$. We assume that each of the grid points is populated by at least one path. This assumption is true in rich scattering such as an urban environment. We now sample the received signal at a rate $f_s = B$, and consider N samples around a reference point (obtained by using the predicted state of the first target) in each pulse repetition interval. The corresponding discrete-time signal is then given by

$$y_{pqm}(nt_s) = \sqrt{\gamma_q \zeta_{pqm}} \sum_{n_f=-\frac{N_f}{2}}^{\frac{N_f}{2}-1} \sum_{n_\tau=0}^{N_\tau-1} \sum_{l=0}^{L-1} \beta_{pqm}^{n_f n_\tau}$$
$$\times a_{lq}(nt_s - lt_p - \tilde{\tau}_{pqm} - n_\tau t_s) e^{j2\pi(\nu_{pqm}+n_f \Delta f)lt_p}$$
$$+ w_p(nt_s). \qquad (9)$$

Here $\tilde{\tau}_{pqm} = f_s \tau_{pqm}$ is the delay in the discrete domain. Expressing (9) in a matrix form, we get

$$y_{pqm} = \sqrt{\gamma_q \zeta_{pqm}} \sum_{n_f=-\frac{N_f}{2}}^{\frac{N_f}{2}-1} \sum_{n_\tau=0}^{N_\tau-1}$$
$$\times \beta_{pqm}^{n_f n_\tau} \underbrace{\left(\boldsymbol{\Upsilon}(n_f) \otimes \boldsymbol{\Gamma}(n_\tau) \right) s_q}_{\phi(n_\tau, n_f)} + w_p \quad (10)$$

where

- y_{pqm} is a $LN \times 1$ received signal vector at the pth antenna due to the signal transmitted from the qth antenna and bouncing off the mth target;
- $\boldsymbol{\Upsilon}(n_f)$ is a $L \times L$ Doppler modulation matrix defined as $\text{diag}\{1, e^{j2\pi(\nu_{pqm}+n_f \Delta f)t_p}, \ldots, e^{j2\pi(\nu_{pqm}+n_f \Delta f)(L-1)t_p}\}$;
- $\boldsymbol{\Gamma}(n_\tau)$ is a $N \times G$ time shift matrix defined as $\left[\mathbf{0}_{(\tilde{\tau}_{pqm}+n_\tau) \times G} \ \boldsymbol{I}_G \ \mathbf{0}_{(N-G-\tilde{\tau}_{pqm}-n_\tau) \times G} \right]^T$;
- s_q is a $LG \times 1$ column vector obtained by stacking the transmitted signal in each pulse from the qth antenna, i.e., $s_q = \left[a_{0q}^T, a_{1q}^T, \ldots, a_{L-1q}^T \right]^T, a_{lq} = \left[a_{lq}^0, \ldots, a_{lq}^{G-1} \right]^T$;
- w_p is a $LN \times 1$ complex additive white Gaussian noise at the pth receiver with zero mean and covariance matrix $\boldsymbol{\Sigma}_{w,p} = \sigma_{w,p}^2 \boldsymbol{I}_{LN}$.

In obtaining (10), we assumed that all the samples of the received waveform $y_{pqm}(t)$ fall within the sampling window of size N and that the pulsewidth is greater than t_s seconds. The

second assumption ensures that there is at least one sample from each pulse. By further simplifying (10), we get

$$y_{pqm} = \sqrt{\gamma_q \zeta_{pqm}} \boldsymbol{\Phi}_{pqm} \boldsymbol{\beta}_{pqm} + w_p \qquad (11)$$

where

- $\boldsymbol{\Phi}_{pqm}$ is a $LN \times N_\tau N_f$ matrix defined as $\boldsymbol{\Phi}_{pqm} = [\ldots, \boldsymbol{\phi}(n_\tau, n_f), \ldots]$;
- $\boldsymbol{\beta}_{pqm}$ is a $N_\tau N_f \times 1$ vector defined as $[\ldots, \beta_{pqm}^{n_\tau n_f}, \ldots]^T$.

The received signal at the pth antenna due to all the targets and all the antennas is then given as

$$y_p = \sum_{q=1}^P \sum_{m=1}^M \sqrt{\gamma_q \zeta_{pqm}} \boldsymbol{\Phi}_{pqm} \boldsymbol{\beta}_{pqm} + w_p. \qquad (12)$$

The final measurement equation is obtained by concatenating the measurement vectors at all the antennas and is given as

$$y = \boldsymbol{\Phi} \boldsymbol{\beta} + w \qquad (13)$$

where

- $y = [y_1^T, \ldots, y_P^T]^T$ is a $LNP \times 1$ vector of the received signal;
- $\boldsymbol{\Phi} = \text{blkdiag}\{\boldsymbol{\Phi}_1, \ldots, \boldsymbol{\Phi}_p, \ldots, \boldsymbol{\Phi}_P\}$ is a $LNP \times PMPN_\tau N_f$ matrix, where $\boldsymbol{\Phi}_p = \{\sqrt{\gamma_1 \zeta_{p11}} \boldsymbol{\Phi}_{p11}, \ldots, \sqrt{\gamma_P \zeta_{pPM}} \boldsymbol{\Phi}_{pPM}\}$;
- $\boldsymbol{\beta} = [\boldsymbol{\beta}_{111}^T, \ldots, \boldsymbol{\beta}_{PPM}^T]^T$ is a $PMPN_\tau N_f \times 1$ vector of the channel state;
- $w = [w_1^T, \ldots, w_P^T]^T$ is a $LNP \times 1$ measurement noise vector with covariance matrix $\boldsymbol{\Sigma}_w = \text{blkdiag}\{\boldsymbol{\Sigma}_{w,1}, \ldots, \boldsymbol{\Sigma}_{w,P}\}$.

B. State Space Model

We denote by $\boldsymbol{\theta}_{m,k}$ the state vector corresponding to the mth target at time k, i.e., $\boldsymbol{\theta}_{m,k} = [x_m, y_m, \dot{x}_m, \dot{y}_m]_k^T$. The dynamics of the mth target at time k are described by

$$\boldsymbol{\theta}_{m,k} = \boldsymbol{F}_{m,\theta} \boldsymbol{\theta}_{m,k-1} + \boldsymbol{v}_{m,\theta} \qquad (14)$$

where $\boldsymbol{F}_{m,\theta}$ is the state transition matrix. We assume that all the targets follow linear trajectories, and hence the state transition matrices are given as

$$\boldsymbol{F}_{m,\theta} = \begin{bmatrix} 1 & 0 & \Delta t & 0 \\ 0 & 1 & 0 & \Delta t \\ 0 & 0 & 1 & 0 \\ 0 & 0 & 0 & 1 \end{bmatrix} \text{ for } m = 1, 2, \ldots, M. \quad (15)$$

Here, Δt is the system sampling time, which corresponds to the time interval after which the processing is done and we refer to it as tracking interval, $\boldsymbol{v}_{m,\theta}$ denotes the error in the state model which is assumed to be Gaussian distributed, with a zero mean and a covariance matrix given by [21]

$$\boldsymbol{\Sigma}_{m,v_\theta} = \epsilon_m \begin{bmatrix} \frac{1}{3}\Delta t^3 & 0 & \frac{1}{2}\Delta t^2 & 0 \\ 0 & \frac{1}{3}\Delta t^3 & 0 & \frac{1}{2}\Delta t^2 \\ \frac{1}{2}\Delta t & 0 & \Delta t & 0 \\ 0 & \frac{1}{2}\Delta t & 0 & \Delta t \end{bmatrix} \qquad (16)$$

where ϵ_m is the intensity of the noise for the mth target. Note that although we assume linear trajectories for all the targets, this assumption is not required. The proposed system will work even if the trajectories of the targets are nonlinear. By concatenating the state vectors of all the targets, we get an overall target state transition equation given as

$$\boldsymbol{\theta}_k = \boldsymbol{F}_\theta \boldsymbol{\theta}_{k-1} + \boldsymbol{v}_\theta \qquad (17)$$

where
- $\boldsymbol{\theta}_k = \left[\boldsymbol{\theta}_{1,k}^T, \ldots, \boldsymbol{\theta}_{M,k}^T\right]^T$ is the $4M \times 1$ vector of the joint target state;
- $\boldsymbol{F}_\theta = \text{blkdiag}\{\boldsymbol{F}_{1,\theta}, \ldots \boldsymbol{F}_{M,\theta}\}$ is the $4M \times 4M$ block diagonal matrix representing the overall state transition matrix;
- $\boldsymbol{v}_\theta = \left[\boldsymbol{v}_{1,\theta}^T, \ldots, \boldsymbol{v}_{M,\theta}^T\right]^T$ is the $4M \times 1$ vector of additive white Gaussian noise with covariance matrix $\boldsymbol{\Sigma}_{v_\theta} = \text{blkdiag}\{\boldsymbol{\Sigma}_{1,v_\theta}, \ldots, \boldsymbol{\Sigma}_{M,v_\theta}\}$.

The state transition for the channel is assumed to be a first order Markovian process, and it is described by the following equation:

$$\boldsymbol{\beta}_k = \boldsymbol{\beta}_{k-1} + \boldsymbol{v}_{\beta,k-1} \qquad (18)$$

where the noise is assumed to be white Gaussian, with a known covariance matrix $\boldsymbol{\Sigma}_{v_\beta}$, given by

$$\boldsymbol{\Sigma}_{v_\beta} = \text{diag}\{\text{vec}(\boldsymbol{\Sigma}_\beta)\} \otimes \boldsymbol{I}_{MN_\tau N_f} \qquad (19)$$

where $\boldsymbol{\Sigma}_\beta$ is a $P \times P$ matrix with $[\boldsymbol{\Sigma}_\beta]_{pq}$ denoting the variance of the mutipath channel between the pth radar and q^{th} radar, and $\text{diag}\{\text{vec}(\boldsymbol{\Sigma}_\beta)\}$ is a $P^2 \times P^2$ diagonal matrix with $\text{vec}(\boldsymbol{\Sigma}_\beta)$ along the principal diagonal. We form an extended state vector by concatenating the target state vector and the channel state vector into a single vector of dimension $4M + PMPN_\tau N_f$ defined as $\boldsymbol{\xi} = [\boldsymbol{\theta}^T, \boldsymbol{\beta}^T]^T$. The state transition equation for $\boldsymbol{\xi}$ is given as

$$\boldsymbol{\xi}_k = \boldsymbol{F}\boldsymbol{\xi}_{k-1} + \boldsymbol{v}_{\xi,k-1} \qquad (20)$$

where the overall state transition matrix is given as

$$\boldsymbol{F} = \begin{bmatrix} \boldsymbol{F}_\theta & \boldsymbol{0}_{4M \times PMPN_\tau N_f} \\ \boldsymbol{0}_{PMPN_\tau N_f \times 4M} & \boldsymbol{I}_{PMPN_\tau N_f} \end{bmatrix}$$

and $\boldsymbol{v}_{\xi,k-1}$ is the additive white Gaussian noise with covariance matrix $\boldsymbol{\Sigma}_{v_\xi}$. Henceforth, when we say state vector, we refer to the extended state vector formed by concatenating the target state and the channel state.

III. TARGET TRACKING BASED ON SEQUENTIAL BAYESIAN INFERENCE

As stated in Section I, a cognitive radar is characterized by a Bayesian tracker at the receiver. Unlike conventional tracking algorithms that perform hard decisions, a Bayesian tracker incorporates information from the past to perform the state estimation at the present time. In this way, the radar receiver continuously learns from its interactions with the environment and uses this experience to enhance its performance. Under the standard

Bayesian framework, the receiver estimates the posterior probability distribution of the state vector, given the past measurements and the current measurement. Let $\boldsymbol{y}_{1:k} = \{\boldsymbol{y}_1, \boldsymbol{y}_2 \ldots \boldsymbol{y}_k\}$ denote the measurements received up to time k. The prediction and the update equation for the target state at time k are given by the Chapman–Kolmogorov equation and Bayes' theorem, respectively:

$$p(\boldsymbol{\xi}_k \mid \boldsymbol{y}_{1:k-1}) = \int p(\boldsymbol{\xi}_k \mid \boldsymbol{\xi}_{k-1}) p(\boldsymbol{\xi}_{k-1} \mid \boldsymbol{y}_{1:k-1}) \text{d}\boldsymbol{\xi}_{k-1} \qquad (21)$$

and

$$p(\boldsymbol{\xi}_k | \boldsymbol{y}_{1:k}) = \frac{1}{z} p(\boldsymbol{y}_k \mid \boldsymbol{\xi}_k) p(\boldsymbol{\xi}_k \mid \boldsymbol{y}_{1:k-1}) \qquad (22)$$

where z is a normalization constant. Using (21), the filter uses the posterior distribution at time $k-1$ to predict the state distribution at time k. Then, using (22), it updates the posterior distribution based on the likelihood function evaluated at time k when the new measurement y_k arrives. In this way, the filter can operate in a sequential manner by updating the posterior distribution. When the measurement and the state transition equations are linear and Gaussian, the optimal Bayesian filter is the Kalman filter [22]. However, for the target-tracking problem, the measurement equation is nonlinear, and evaluating a closed form expression for the posterior distribution of the state vector is not feasible.

A. Standard Particle Filter

One of the most commonly used suboptimal Bayesian filters that can be employed in a nonlinear scenario is a particle filter [23], [24]. A standard particle filter (SPF) computes a discrete weighted approximation to the true posterior distribution, using

$$p(\boldsymbol{\xi}_k \mid \boldsymbol{y}_{1:k}) \approx \sum_{i=1}^{N_s} w_k^{(i)} \delta(\boldsymbol{\xi}_k - \boldsymbol{\xi}_k^{(i)}) \qquad (23)$$

where $\left\{\boldsymbol{\xi}_k^{(i)}\right\}_{i=1}^{N_s}$ are the support points (or samples) that characterize the probability distribution $p(\boldsymbol{\xi}_k|\boldsymbol{y}_{1:k})$, and $\left\{w_k^{(i)}\right\}_{i=1}^{N_s}$ are the associated weights. The samples $\left\{\boldsymbol{\xi}_k^{(i)}\right\}_{j=1}^{N_s}$ are drawn from a known proposal distribution, and the weights are derived using the principle of importance sampling [25]. In general, the proposal distribution is chosen to be the transitional prior. This choice results in a simple weight update equation given as

$$\tilde{\boldsymbol{w}}_k^{(i)} \propto \boldsymbol{w}_{k-1}^{(i)} p\left(\boldsymbol{y}_k \mid \boldsymbol{\xi}_k^{(i)}, \boldsymbol{y}_{1:k-1}\right) \qquad (24)$$

where $\tilde{\boldsymbol{w}}_k^{(i)}$ is un-normalized weight of ith particle at time k. Standard particle filters, based on the principle of importance sampling, suffer from a drawback called the degeneracy phenomenon. After a few iterations, the weights of all but a few particles will be close to zero. As a result of degeneracy, the number of particles contributing to the posterior distribution become significantly less over time, and hence the performance of the filter degrades. In theory, it is impossible to avoid degeneracy, but its effect can be reduced by using a large number of

particles. However, the number of particles required to approximate the posterior density using a discrete measure, grows exponentially [26] with the dimension of the state vector. Filters using such large number of particles are computationally complex and run into numerical inconsistencies. For the problem of joint estimation of target and channel states, the state vector is of high dimension and hence standard particle filters are not suitable.

B. Multiple Rao–Blackwell Particle Filter

We propose a new hybrid filter that partitions the state space into lower dimensional subspaces and generates the particles from the lower dimensional state space. Our method is based on the combination of a multiple particle filter [27] and a Rao–Blackwellized particle filter [28]–[30]. The idea behind a multiple particle filter is to partition the state space into subspaces of lower dimension, such that the state transition of each subspace is independent of other subspaces, and then to employ multiple particle filters operating on each subspace independently. The idea behind a Rao–Blackwellized particle filter is to partition the state space, such that conditioned on one partition the system becomes linear and Gaussian. This partition can then be marginalized out analytically using a Kalman filter. The Rao-Blackwell theorem states that the variance of the estimates obtained after Rao–Blackwellization is less than the variance of the original estimate. We use these ideas to develop a hybrid filter which is a combination of both MPF and a RBPF. We first partition the state space as target state and channel state, i.e., $\boldsymbol{\xi} = [\boldsymbol{\theta}^T, \boldsymbol{\beta}^T]^T$. The joint posterior distribution at time k, given the measurements up to k can be expressed as

$$p(\boldsymbol{\xi}_k | \boldsymbol{y}_{1:k}) = p(\boldsymbol{\beta}_k | \boldsymbol{\theta}_k, y_{1:k}) \, p(\boldsymbol{\theta}_k | \boldsymbol{y}_{1:k}). \tag{25}$$

Given a particle $\boldsymbol{\theta}_k^{(i)}$, the measurement model given in (13), is linear and Gaussian in the channel state vector $\boldsymbol{\beta}$. Hence, we use a Kalman filter to obtain the measurement and time updates corresponding to the partition $\boldsymbol{\beta}$. Next, we further partition the target state into smaller subspaces where each partition corresponds to the state of a single target. Since the state transition corresponding to each target is independent of other targets, the distribution $p(\boldsymbol{\theta}_k | \boldsymbol{y}_{1:k})$ can be expressed as

$$p(\boldsymbol{\theta}_k | \boldsymbol{y}_{1:k}) = \prod_{m=1}^{M} p(\boldsymbol{\theta}_{m,k} | \boldsymbol{y}_{1:k}). \tag{26}$$

We employ one particle filter for each partition, and approximate the distributions $p(\boldsymbol{\theta}_{m,k} | \boldsymbol{y}_{1:k}), m = 1, \ldots, M$ using random measures defined by $(\boldsymbol{\theta}_{m,k}^{(i)}, w_{m,k}^{(i)})$. The corresponding weight update equations can be expressed as [27]

$$\tilde{w}_{m,k}^{(i)} \propto w_{m,k-1}^{(i)} p\left(\boldsymbol{y}_k | \boldsymbol{\theta}_{m,k}^{(i)}, \boldsymbol{y}_{1:k-1}\right). \tag{27}$$

The density $p(\boldsymbol{y}_k | \boldsymbol{\theta}_{m,k}^{(i)}, \boldsymbol{y}_{1:k-1}) \neq p(\boldsymbol{y}_k | \boldsymbol{\theta}_{m,k}^{(i)})$ since the measurements $\boldsymbol{y}_{1:k-1}$ contain the information about the channel state $\boldsymbol{\beta}_k$ and the target state

$\boldsymbol{\theta}_{-m,k} = [\boldsymbol{\theta}_1, \ldots, \boldsymbol{\theta}_{m-1}, \boldsymbol{\theta}_{m+1}, \ldots, \boldsymbol{\theta}_M]_k^T$. We express the distribution $p(\boldsymbol{y}_k | \boldsymbol{\theta}_{m,k}^{(i)}, \boldsymbol{y}_{1:k-1})$ as

$$\begin{aligned} p(\boldsymbol{y}_k | \boldsymbol{\theta}_{m,k}^{(i)}, \boldsymbol{y}_{1:k-1}) = \int & p(\boldsymbol{y}_k | \boldsymbol{\theta}_{m,k}^{(i)}, \boldsymbol{\theta}_{-m,k}, \boldsymbol{\beta}_k) \\ & \times p(\boldsymbol{\beta}_k | \boldsymbol{\theta}_{m,k}^{(i)}, \boldsymbol{y}_{1:k-1}) \\ & \times p(\boldsymbol{\theta}_{-m,k} | \boldsymbol{\theta}_{m,k}^{(i)}, \boldsymbol{y}_{1:k-1}) \mathrm{d}\boldsymbol{\beta}_k \mathrm{d}\boldsymbol{\theta}_{-m,k}, \end{aligned} \tag{28}$$

and the distributions $p(\boldsymbol{\beta}_k | \boldsymbol{\theta}_{m,1:k}^{(i)}, \boldsymbol{y}_{1:k-1})$ and $p(\boldsymbol{\theta}_{-m,k} | \boldsymbol{\theta}_{m,k}^{(i)}, \boldsymbol{y}_{1:k-1})$ as

$$p(\boldsymbol{\beta}_k | \boldsymbol{\theta}_{m,k}^{(i)}, \boldsymbol{y}_{1:k-1}) = \int p(\boldsymbol{\beta}_k | \boldsymbol{\beta}_{k-1}) p(\boldsymbol{\beta}_{k-1} | \boldsymbol{y}_{1:k-1}) \mathrm{d}\boldsymbol{\beta}_{k-1} \tag{29}$$

and

$$\begin{aligned} & p(\boldsymbol{\theta}_{-m,k} | \boldsymbol{\theta}_{m,k}^{(i)}, \boldsymbol{y}_{1:k-1}) \\ & = \prod_{\substack{n=1 \\ n \neq m}}^{M} \int p(\boldsymbol{\theta}_{n,k} | \boldsymbol{\theta}_{n,k-1}) p(\boldsymbol{\theta}_{n,k-1} | \boldsymbol{y}_{1:k-1}) \mathrm{d}\boldsymbol{\theta}_{n,k-1}. \end{aligned} \tag{30}$$

We identify (29) and (30) to be the time update equations corresponding to the Kalman filter and the $M - 1$ particle filters, respectively. Also, (29) can be computed analytically since the distributions defined in this equation are Gaussian [29]. Following the similar procedure, we compute the weight update equations corresponding to all M particle filters. Finally, we compute the marginal $p(\boldsymbol{\beta}_k | y_{1:k})$ using

$$p(\boldsymbol{\beta}_k | y_{1:k}) = \int p(\boldsymbol{\beta}_k | \boldsymbol{\theta}_k, y_{1:k}) \times p(\boldsymbol{\theta}_k | y_{1:k}) \mathrm{d}\boldsymbol{\theta}_k. \tag{31}$$

It can be shown that $\boldsymbol{\beta}_k | y_{1:k} \sim \mathbb{CN}(\boldsymbol{\beta}_k^+, \boldsymbol{G}_k^+)$, where $\boldsymbol{\beta}_k^+$ and $\boldsymbol{G}_k^+$ are given by the measurement update equations corresponding to the Kalman filter. In this manner, the filter jointly estimates the multiple target positions and velocities, using Monte Carlo based approach with one particle filter per target, and channel state, using a Kalman filter. We refer to this Bayesian filter as multiple Rao–Blackwell particle filter (MRBPF). The overall algorithm is given in Table I.

IV. ANTENNA SCHEDULING AND POWER ALLOCATION

We use the posterior Cramér–Rao bound (PCRB) as an optimization criterion for antenna scheduling and power allocation. The PCRB is a lower bound on the mean-square error (MSE) of the Bayesian estimates of the state vector and hence we seek to find the optimal antenna set and the corresponding power to be transmitted by these antennas by minimizing the PCRB. Another motivation for using the PCRB is that it can be computed in a sequential manner [31] in every interval. The recursive formulation for the computation of PCRB suits the problem of target tracking, where we need to find the estimates of the state vector in every tracking interval, and hence the PCRB is a natural choice for the optimization criterion. The PCRB for the tracking problem is defined and derived as follows.

1	**Initialization:** Start with $\{\boldsymbol{\theta}_{m,0}^{(i)}\}_{i=1}^{N_s}, \boldsymbol{\beta}_0^+$, and $\{\mathbf{G}_0^+\}$. Initialize the weights $w_{m,0}^{(i)} = 1/N_s$ for $m = 1, 2, \cdots M$. Set k = 1. Then for each i
2	Draw the samples $\{\boldsymbol{\theta}_{m,k}^{(i)}\}_{i=1}^{N_s}$ from the proposal distributions $p(\boldsymbol{\theta}_{m,k}|\boldsymbol{\theta}_{m,k-1})$.
3	Compute $\boldsymbol{\Phi}_k^{(i)}$ based on the samples $\{\boldsymbol{\theta}_{m,k}^{(i)}\}_{i=1}^{N_s}, m = 1, \cdots M$
4	**Kalman filter time update:** Compute the Kalman gain and obtain the predicted value of the channel state vector $\boldsymbol{\beta}_k^-$ using the following equations. $$\begin{aligned} \mathbf{G}_k^- &= \boldsymbol{\Sigma}_{v_\beta} + \mathbf{G}_{k-1}^+ \\ \mathbf{P}_k^{(i)} &= \boldsymbol{\Sigma}_w + \boldsymbol{\Phi}_k^{(i)} \mathbf{G}_k^- (\boldsymbol{\Phi}_k^{(i)})^H \\ \mathbf{J}_k^{(i)} &= \mathbf{G}_k^- (\boldsymbol{\Phi}_k^{(i)})^H (\mathbf{P}_k^{(i)})^{-1} \\ \boldsymbol{\beta}_k^- &= \boldsymbol{\beta}_{k-1}^+ \end{aligned}$$
5	**Particle filter time update:** Compute the predicted value of the mth target state using the equation $$\boldsymbol{\theta}_{m,k}^- = \sum_{i=1}^{N_s} w_{m,k-1}^{(i)} \boldsymbol{\theta}_{m,k}^{(i)}$$
6	**Particle filter measurement update:** Compute the unnormalized weights for each m using the equation $$\tilde{w}_{m,k}^{(i)} = w_{m,k-1}^{(i)} p\left(\boldsymbol{y}_k | \boldsymbol{\theta}_{m,k}^{(i)}, \boldsymbol{\theta}_{-m,k}^-, \boldsymbol{\beta}_k^-\right)$$
7	Normalize the weights using $w_{m,k}^{(i)} = \dfrac{\tilde{w}_{m,k}^{(i)}}{\sum_{i=1}^{N_s} \tilde{w}_{m,k}^{(i)}}$
8	**Kalman filter measurement update:** Update the covariance matrix of the channel state and the channel state itself using $$\begin{aligned} \boldsymbol{z}_k^{(i)} &= \boldsymbol{\Phi}_k^{(i)} \boldsymbol{\beta}_k^- \\ \boldsymbol{\beta}_k^+ &= \frac{1}{M} \sum_{m=1}^M \sum_{i=1}^{N_s} w_{m,k}^{(i)} \left(\boldsymbol{\beta}_k^- + \mathbf{J}_k^{(i)}(\boldsymbol{y}_k - \boldsymbol{z}_k^{(i)})\right) \\ \mathbf{G}_k^+ &= \frac{1}{M} \sum_{m=1}^M \sum_{i=1}^{N_s} w_{m,k}^{(i)} (\boldsymbol{I} - \mathbf{J}_k^{(i)} \boldsymbol{\Phi}_k^{(i)}) \mathbf{G}_k^- \end{aligned}$$
9	Obtain the estimates of the target states using the equation $$\hat{\boldsymbol{\theta}}_{m,k} = \sum_{i=1}^{N_s} w_{m,k}^{(i)} \boldsymbol{\theta}_{m,k}^{(i)}$$
10	**Resampling:** Depending on the weights $w_{m,k}^{(i)}$, resample the set $\{\boldsymbol{\theta}_{m,k}^{(i)}\}_{i=1}^{N_s}$ to obtain new particles

A. Computation of the Posterior Cramér Rao Bound

Let $\Delta_{\boldsymbol{\eta}} = [\partial\eta_1, \partial\eta_2, \ldots \partial\eta_r]^T$ denote a vector of the partial derivatives with respect to the vector $\boldsymbol{\eta}$ and $\Delta_v^\kappa = \Delta_v \Delta_\kappa^T$ denote the partial derivative vectors. With this notation, the PCRB for an unbiased estimate of $\boldsymbol{\xi}$ has the form

$$\mathbb{E}[(\boldsymbol{\xi} - \hat{\boldsymbol{\xi}})(\boldsymbol{\xi} - \hat{\boldsymbol{\xi}})^T] \geq \boldsymbol{J}^{-1} \qquad (32)$$

where $\boldsymbol{J}$ is the Fisher information matrix (FIM), given as

$$\boldsymbol{J} = -\mathbb{E}\left[\Delta_\xi^\xi \log\left(p(\boldsymbol{\xi}, \boldsymbol{y})\right)\right]. \qquad (33)$$

The recursive equation to compute the FIM in an online and recursive manner was proposed in [31], and we state it here for completeness.

Theorem 1: The sequence $\{\boldsymbol{J}_k\}$ of posterior information submatrices for estimating state vector obeys the recursion

$$\boldsymbol{J}_{k+1} = D_k^{22} - D_k^{21}(\boldsymbol{J}_k + D_n^{11})^{-1} D_k^{12} \qquad (34)$$

where

$$D_k^{11} = \mathbb{E}\left\{-\Delta_{\xi_k}^{\xi_k} \log p(\boldsymbol{\xi}_{k+1}|\boldsymbol{\xi}_k)\right\}$$

$$D_k^{12} = \mathbb{E}\left\{-\Delta_{\xi_{k+1}}^{\xi_k} \log p(\boldsymbol{\xi}_{k+1}|\boldsymbol{\xi}_k)\right\}$$

$$D_k^{21} = \mathbb{E}\left\{-\Delta_{\xi_k}^{\xi_{k+1}} \log p(\boldsymbol{\xi}_{k+1}|\boldsymbol{\xi}_k)\right\}$$

and

$$\begin{aligned} D_k^{22} &= \mathbb{E}\left\{-\Delta_{\xi_{k+1}}^{\xi_{k+1}} \log p(\boldsymbol{\xi}_{k+1}|\boldsymbol{\xi}_k)\right\} \\ &\quad + \mathbb{E}\left\{-\Delta_{\xi_{k+1}}^{\xi_{k+1}} \log p(\boldsymbol{y}_{k+1}|\boldsymbol{\xi}_{k+1})\right\}, \end{aligned}$$

and the expectation is taken with respect to the joint distribution $p(\boldsymbol{\xi}_{k+1}, \boldsymbol{y}_{k+1})$.

From (20), $p(\boldsymbol{\xi}_{k+1}|\boldsymbol{\xi}_k) \sim \mathcal{N}(\boldsymbol{F}\boldsymbol{\xi}_k, \boldsymbol{\Sigma}_{v_\xi})$. With this substitution and using the matrix-inversion lemma, it can be shown that (34) reduces to

$$\boldsymbol{J}_{k+1} = \left[\boldsymbol{\Sigma}_{v_\xi} + \boldsymbol{F}\boldsymbol{J}_k^{-1}\boldsymbol{F}^T\right]^{-1} + \boldsymbol{\Gamma}_{k+1} \qquad (35)$$

where

$$\boldsymbol{\Gamma}_{k+1} = \mathbb{E}\left[-\Delta_{\xi_{k+1}}^{\xi_{k+1}} \log p(\boldsymbol{y}_{k+1}|\boldsymbol{\xi}_{k+1})\right]. \qquad (36)$$

Since the estimate of the state vector, $\boldsymbol{\xi}_{k+1}$, is not available at time k, the term $\boldsymbol{\Gamma}_{k+1}$ does not have a closed form expression.

TABLE II
TABLE SHOWING THE GREEDY ALGORITHM FOR SENSOR SCHEDULING AND POWER ALLOCATION

1	**First Pass:**
(i)	Initialize $\pi_{k+1} = \{1\}$
(ii)	For each antenna i, compute $e_i = \text{trace}(\mathbf{J}_{k+1}^{-1})$, using Eqs. (35), (37), and (38), with $\pi_{k+1} = \{1, i\}$ and $\gamma_{k+1} = \frac{\eta_e}{P}$
(iii)	Compute the distance between the ith antenna and the first antenna using $d_i = \sqrt{(x_i^2 + y_i^2)}$
(iv)	Compute the product $v_i = d_i \times e_i$ and sort the antennas in decreasing order of v_i
(v)	Select the antennas sequentially in the above order, and add them to π_{k+1} until there are no more antennas left or an antenna j does not satisfy the distance constraint, i.e., until $$d_j > \eta_c - \sum_{i=1}^{j-1} d_i \qquad (42)$$
(vi)	If $e_j > e_{\pi_{k+1}}$, where $e_{\pi_{k+1}} = \text{trace}(\mathbf{J}_{k+1}^{-1})$, with π_{k+1}, choose $\pi_{k+1}^* = \pi_{k+1}$, otherwise, choose $\pi_{k+1}^* = \{1, j\}$
2	**Second Pass:**
(i)	For each antenna, $i \in \pi_{k+1}^*$, compute the ratio $$\lambda_i = \sum_{p \in \pi_{k+1}^*} \frac{\sum_{m=1}^M \zeta_{ipm}[\boldsymbol{\Sigma}_\beta]_{ip}}{\sigma_{w,p}^2} \qquad (43)$$
(ii)	Choose the energy to be transmitted on the ith antenna as $$\gamma_{i,k+1}^* = \frac{\lambda_i \eta_e}{\sum_{j \in \pi_{k+1}^*} \lambda_j} \qquad (44)$$
3	**Update FIM**
(i)	Update $\mathbf{J}_{k+1}$ using Eqs. (35), (37), and (38), using π_{k+1}^* and $\boldsymbol{\gamma}_{k+1}^*$

We use Monte Carlo sampling to obtain an approximate value, outlined as follows:

$$\boldsymbol{\Gamma}_{k+1} = \mathbb{E}\left[-\Delta_{\xi_{k+1}}^{\xi_{k+1}} \log p(\boldsymbol{y}_{k+1}|\boldsymbol{\xi}_{k+1})\right]$$

$$= \mathbb{E}_\xi\left[\mathbb{E}_{\boldsymbol{y}|\xi}\left[-\Delta_{\xi_{k+1}}^{\xi_{k+1}} \log p(\boldsymbol{y}_{k+1}|\boldsymbol{\xi}_{k+1})\right]\right]$$

$$\approx \frac{1}{M} \sum_{i=1}^{N_s} \sum_{m=1}^{M} w_{m,k}^{(i)} \boldsymbol{\Xi}_{k+1}\left(\boldsymbol{\theta}_{k+1}^{(i)}, \boldsymbol{\beta}_{k+1}^{(i)}\right) \qquad (37)$$

where

$$\boldsymbol{\Xi}_{k+1}\left(\boldsymbol{\theta}_{k+1}, \boldsymbol{\beta}_{k+1},\right) = \mathbb{E}_{\boldsymbol{y}|\xi}\left[-\Delta_{\xi_{k+1}}^{\xi_{k+1}} \log p(\boldsymbol{y}_{k+1}|\boldsymbol{\xi}_{k+1})\right],$$

$\boldsymbol{\xi}_{k+1} = \left[\boldsymbol{\theta}_{k+1}^T, \boldsymbol{\beta}_{k+1}^T\right]^T$, and $\boldsymbol{\theta}_{k+1}^{(i)}$ and $\boldsymbol{\beta}_{k+1}^{(i)}$ are the samples drawn from the state transition functions of the target state and channel state vectors following (17) and (18), respectively. The value of $\boldsymbol{\Xi}_{k+1}\left(\boldsymbol{\theta}_{k+1}, \boldsymbol{\beta}_{k+1},\right)$ is stated in the following theorem and derived in the Appendix.

Theorem 2: Let $\pi_k \subseteq \{1, 2, \ldots N\}$ denote the set of the radars that are in operation at time k. For the measurement model described in (13), we have

$$\boldsymbol{\Xi}_{k+1}\left(\boldsymbol{\theta}_{k+1}, \boldsymbol{\beta}_{k+1},\right)$$

$$= 2 \sum_{p,q,r \in \pi_{k+1}} \sqrt{\gamma_q \gamma_r} \Re\left\{\left(\frac{\partial \boldsymbol{\mu}_{k+1}^{pq}}{\partial \boldsymbol{\xi}_{k+1}}\right) \boldsymbol{\Sigma}_{w,p}^{-1} \left(\frac{\partial \boldsymbol{\mu}_{k+1}^{pr}}{\partial \boldsymbol{\xi}_{k+1}}\right)^H\right\} \qquad (38)$$

where $\boldsymbol{\mu}_{k+1}^{pq} = \sum_{m=1}^M \sqrt{\zeta_{pqm}} \boldsymbol{\Phi}_{pqm,k+1} \boldsymbol{\beta}_{pqm,k+1}$, and the expressions for $\frac{\partial \boldsymbol{\mu}_{k+1}^{pq}}{\partial \boldsymbol{\xi}_{k+1}}$ are derived in the Appendix.

B. Approximate Greedy Algorithm for Adaptive Antenna Scheduling and Power Allocation

Our approach to antenna scheduling and power allocation for the radar network is based on the minimization of the predicted value of the PCRB, under suitable constraints. The constraints represent the bounds on the total power and total cost available for deploying the antennas. In general, the cost of communicating the information from a radar to the fusion center is proportional to the distance between them. Hence, we use the Euclidean distance measure as an indicator of the communication cost. We devise the following constrained joint optimization problem for scheduling and power allocation.

$$\boldsymbol{\pi}_{k+1}^*, \boldsymbol{\gamma}_{k+1}^* = \arg\min_{\Pi,\Gamma} \text{trace}(\boldsymbol{J}_{k+1})^{-1} \text{ subject to} \qquad (39)$$

$$\sum_{p \in \pi_{k+1}} \sqrt{(x_p^2 + y_p^2)} \leq \eta_c \qquad (40)$$

and

$$\sum_{p \in \pi_{k+1}} \gamma_p \leq \eta_e. \qquad (41)$$

The first constraint in the problem represents the communication cost constraint and second constraint represents the power constraint. The parameters η_c and η_e correspond to the bounds on the total communication cost and the total power. Obtaining a solution to this joint optimization problem is NP-hard. We propose a two pass greedy algorithm to find a suboptimal solution to this problem. We separate the problem into two parts: the problem of finding the antennas to be employed and the problem of finding the power to be allocated to these antennas. In the first pass, we transmit equal power on all the antennas and solve the problem of selecting an optimal set of antennas to be used. To

select an optimal subset of antennas to be used, we can evaluate the FIM over all possible combinations of subsets of antennas, and choose the best one. The complexity of such an evaluation grows exponentially with the number of antennas. We obtain an approximate solution by employing an approximate greedy algorithm whose computational complexity grows linearly with the number of antennas. We compute the FIM for all the antennas separately, and greedily select the ones which minimize the product of the Euclidian distance and the trace of the inverse of the FIM. Once the antennas are selected, in the second pass, we distribute the power to these antennas, again using a greedy approach. In this case, we allocate more power to the antennas that maximize the overall signal-to-noise ratio (SNR). Since the PCRB is inversely related to the SNR [22], we are minimizing by PCRB by maximizing the SNR. The algorithm is summarized below in Table II.

V. NUMERICAL RESULTS

In this section, we use numerical examples to study the performance of the proposed cognitive radar network system in the presence of the time-varying multipath propagation conditions. We demonstrate the advantage of the proposed MRBPF method by comparing it to the SPF. We also demonstrate the advantage of the proposed adaptive antenna scheduling and power allocation methods compared to the fixed antenna scheme and equal power allocation. Finally, we demonstrate the advantage of the multipath modeling. We describe the simulation setup first and then discuss the numerical examples.

Signal and Multipath parameters: We considered OFDM waveforms with eight $(G = 8)$ subcarriers loaded with same symbol in all the subcarriers. The total bandwidth was 100 MHz $(B = 100)$ and the carrier frequency, f_c, of the transmitted waveforms was 1 GHz. We used four $(L = 4)$ pulses in each tracking interval. The multipath environment consisted of delay and Doppler shifts. We used three Doppler shifts and two delay shifts, i.e., $N_\tau = 2$ and $N_f = 3$. The vector $\boldsymbol{\beta}_{pqm}$ was generated from a Gaussian distribution with zero mean and unit variance and scaled later such that variance of the coefficients corresponding to different delays decayed exponentially.

Target and the Radar Network parameters: We considered three different configurations for the target trajectories and the antenna locations for the examples. These configurations are shown in Fig. 2.

In the first configuration, the network consisted of three monostatic radars located at

$$(x_1, y_1) = (0, 0), (x_2, y_2) = (10, 25), (x_3, y_3) = (25, 20).$$

There were two crossing targets $(M = 2)$ moving in the region of interest with the initial position of the first target at $(x_1, y_1) = (5, 5)$ m and that of the second target at $(x_2, y_2) = (30, 10)$ m. The targets were moving with constant velocities of $(\dot{x}_1, \dot{y}_1) = (12, 12)$ m/s and $(\dot{x}_2, \dot{y}_2) = (-15, 15)$ m/s along linear trajectories. The co-variance matrix of the process noise for the target state transition was given by (16) with $\epsilon_1 = \epsilon_2 = 1$. The co-variance matrix of the process noise for the channel state transition was given by (19) with $\boldsymbol{\Sigma}_\beta = \sigma_\beta^2 \boldsymbol{I}_P$, where $\sigma_\beta^2 = 5 \times 10^{-2}$. The variance of the measurement noise at each receiver was $\sigma_{w,p}^2 = 5 \times 10^{-2}, p = 1, \ldots P$.
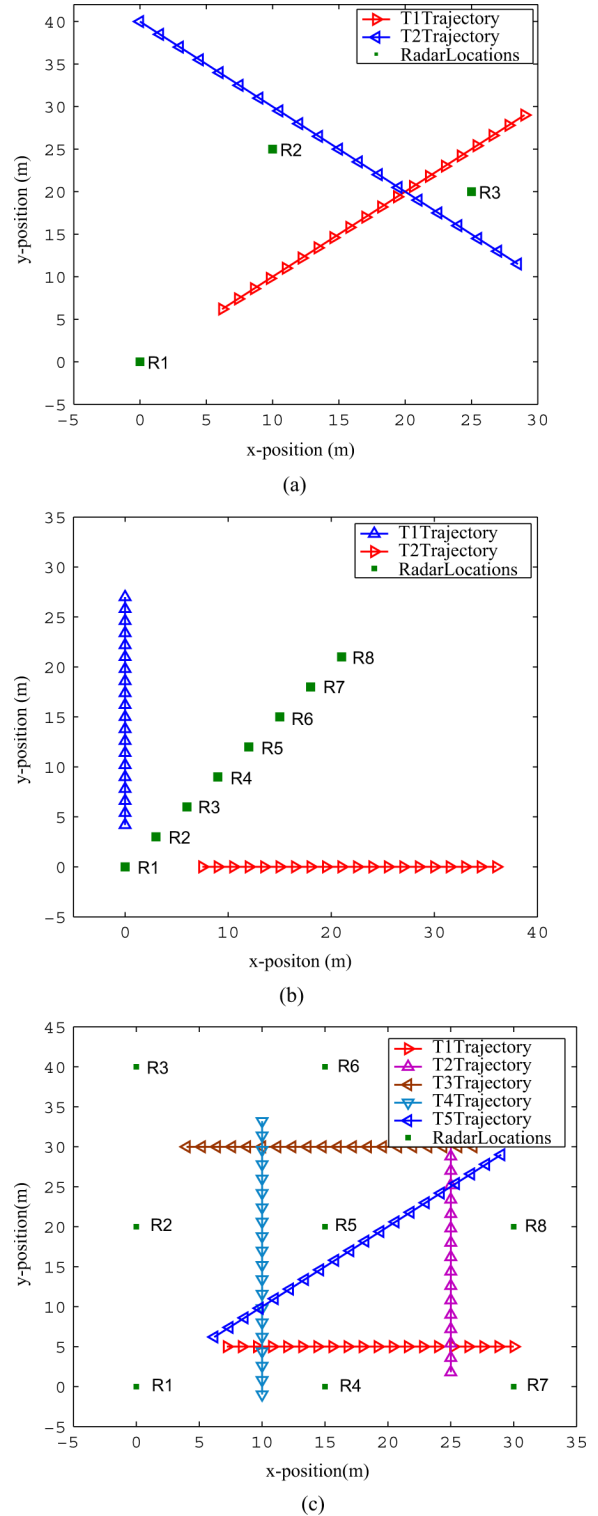

(a)

(b)

(c)

Fig. 2. Three configurations used in the numerical examples (a) First configuration. (b) Second configuration. (c) Third configuration.

In the second configuration, the network consisted of eight monostatic radars located at

$$(x_1, y_1) = (0, 0), (x_2, y_2) = (3, 3), (x_3, y_3)$$
$$= (6, 6), (x_4, y_4) = (9, 9)$$
$$(x_5, y_5) = (12, 12), (x_6, y_6) = (15, 15)$$
$$(x_7, y_7) = (18, 18), (x_8, y_8) = (21, 21).$$

There were two noncrossing targets $(M = 2)$ with the initial position of the first target at $(x_1, y_1) = (0, 3)$ m and the second target at $(x_2, y_2) = (6, 0)$ m. The targets moved with constant velocities of $(\dot{x}_1, \dot{y}_1) = (0, 12)$ m/s and $(\dot{x}_2, \dot{y}_2) = (15, 0)$ m/s along linear trajectories. The co-variance matrix of the process noise for the target state transition was same as the corresponding co-variance matrix used in the first configuration. The co-variance matrix of the process noise for the channel state was given by (19), with

$$\boldsymbol{\Sigma}_\beta =$$
$$\begin{bmatrix} 0.01 & 0.01 & 0.01 & 0.005 & 0.005 & 0.005 & 0.003 & 0.002 \\ 0.01 & 0.01 & 0.01 & 0.005 & 0.005 & 0.005 & 0.003 & 0.002 \\ 0.01 & 0.01 & 0.01 & 0.005 & 0.005 & 0.005 & 0.003 & 0.002 \\ 0.005 & 0.005 & 0.005 & 0.01 & 0.005 & 0.005 & 0.003 & 0.002 \\ 0.005 & 0.005 & 0.005 & 0.005 & 0.01 & 0.005 & 0.003 & 0.002 \\ 0.005 & 0.005 & 0.005 & 0.005 & 0.005 & 0.01 & 0.003 & 0.002 \\ 0.003 & 0.003 & 0.003 & 0.003 & 0.003 & 0.003 & 0.01 & 0.002 \\ 0.002 & 0.002 & 0.002 & 0.002 & 0.002 & 0.002 & 0.002 & 0.01 \end{bmatrix}.$$

The variance of the measurement noise was given by the vector

$$\begin{aligned} \sigma_{\mathrm{w}}^2 &= \left(\sigma_{\mathrm{w},1}^2, \ldots \sigma_{\mathrm{w},P}^2 \right) \\ &= \left(5 \times 10^{-2}, 5 \times 10^{-2}, 3 \times 10^{-2}, 3 \times 10^{-2}, \right. \\ &\quad \left. 5 \times 10^{-2}, 2 \times 10^{-2} 2 \times 10^{-2}, 1 \times 10^{-2} \right). \end{aligned}$$

In the third configuration, the network consisted of nine radars located at

$$\begin{aligned} (x_1, y_1) &= (0, 0), (x_2, y_2) = (0, 20) \\ (x_3, y_3) &= (0, 40), (x_4, y_4) = (15, 0) \\ (x_5, y_5) &= (15, 20), (x_6, y_6) = (15, 40) \\ (x_7, y_7) &= (30, 0), (x_8, y_8) = (30, 20) \\ (x_9, y_9) &= (30, 40). \end{aligned}$$

There were five crossing targets $(M = 5)$ with the initial position of targets at $(x_1, y_1) = (6, 5)$ m, $(x_2, y_2) = (25, 0)$ m, $(x_3, y_3) = (28, 30)$ m, $(x_4, y_4) = (10, 35)$ m, $(x_5, y_5) = (5, 5)$ m, respectively. The targets moved with constant velocities of $(\dot{x}_1, \dot{y}_1) = (12, 0)$ m/s, $(\dot{x}_2, \dot{y}_2) = (0, 18)$ m/s, $(\dot{x}_3, \dot{y}_3) = (-12, 0)$ m/s, $(\dot{x}_4, \dot{y}_4) = (0, -18)$ m/s, and $(\dot{x}_5, \dot{y}_5) = (12, 12)$ m/s, respectively, along linear trajectories. The co-variance matrix of the process noise for the target state transition was same as the one used for the first two configurations and the co-variance matrix of the process noise for the channel state was given by (19), with $\boldsymbol{\Sigma}_\beta = \sigma_\beta^2 \boldsymbol{I}_P$, where $\sigma_\beta^2 = 5 \times 10^{-2}$. The variance of the measurement noise was given by the vector

$$\begin{aligned} \sigma_{\mathrm{w}}^2 &= \left(\sigma_{\mathrm{w},1}^2, \ldots \sigma_{\mathrm{w},P}^2 \right) \\ &= \left(5 \times 10^{-2}, 3 \times 10^{-2}, 5 \times 10^{-2}, 3 \times 10^{-1}, 1 \times \right. \\ &\quad \left. 10^{-2}, 3 \times 10^{-2} 5 \times 10^{-2}, 3 \times 10^{-1}, 5 \times 10^{-1} \right). \end{aligned}$$

In all the examples, the tracking interval length was chosen to be 0.1 seconds and the motion of the targets over 20 tracking intervals was considered. The parameter η_{e} was chosen to be
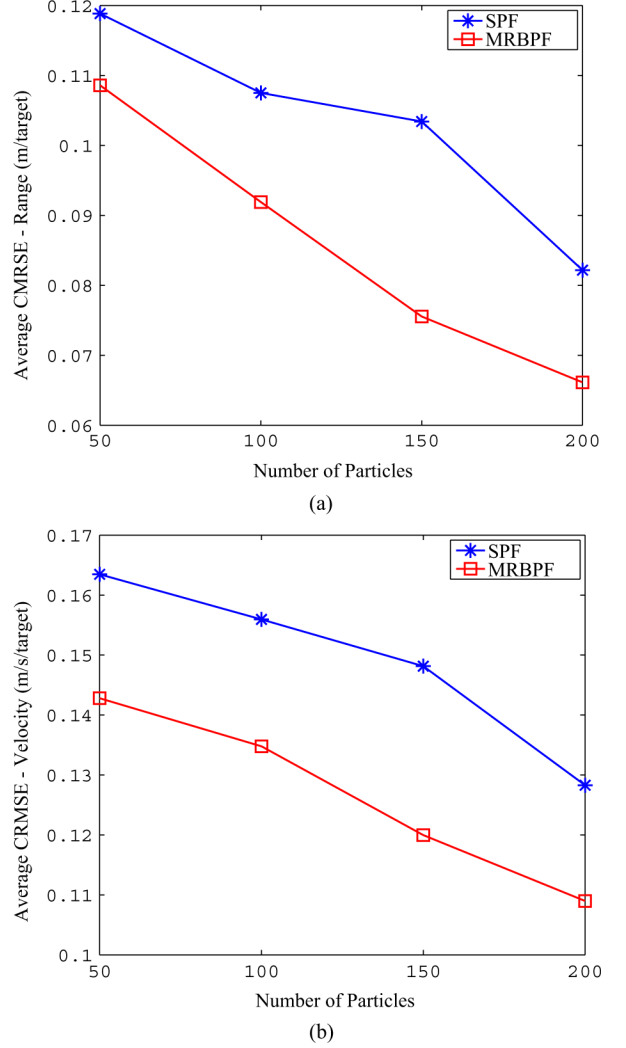

Fig. 3. Average CRMSE of the range and the velocity estimates plotted against the number of particles for the SPF and the MRBPF. (a) CRMSE in range. (b) CRMSE in velocity.

120, which corresponds to the total transmit power constraint. The simulations were averaged over 100 Monte Carlo iterations $(N_{\mathrm{mc}} = 100)$. In order to analyze the performance improvement due to the adaptive scheduling and power allocation methods, we plot the composite root mean-squared error (CRMSE) versus the tracking interval index. We define the CMRSE in the range and velocity estimates, respectively, as

$$\begin{aligned} &\mathrm{CRMSE}_{\mathrm{ran}} \\ &= \frac{1}{MN_{\mathrm{mc}}} \sum_{i=1}^{N_{\mathrm{mc}}} \sum_{m=1}^{M} \sqrt{(x_m - \hat{x}_{m,i})^2 + (y_m - \hat{y}_{m,i})^2} \\ &\mathrm{CRMSE}_{\mathrm{vel}} \\ &= \frac{1}{MN_{\mathrm{mc}}} \sum_{i=1}^{N_{\mathrm{mc}}} \sum_{m=1}^{M} \sqrt{(\dot{x}_m - \hat{\dot{x}}_{m,i})^2 + (\dot{y}_m - \hat{\dot{y}}_{m,i})^2} \quad (45) \end{aligned}$$

where $[\hat{x}_{m,i}, \hat{y}_{m,i}, \hat{\dot{x}}_{m,i}, \hat{\dot{y}}_{m,i}]^T$ is the estimate of the mth target state in the ith Monte Carlo run, and $[x_m, y_m, \dot{x}_m, \dot{y}_m]^T$ is the actual m^{th} target state.
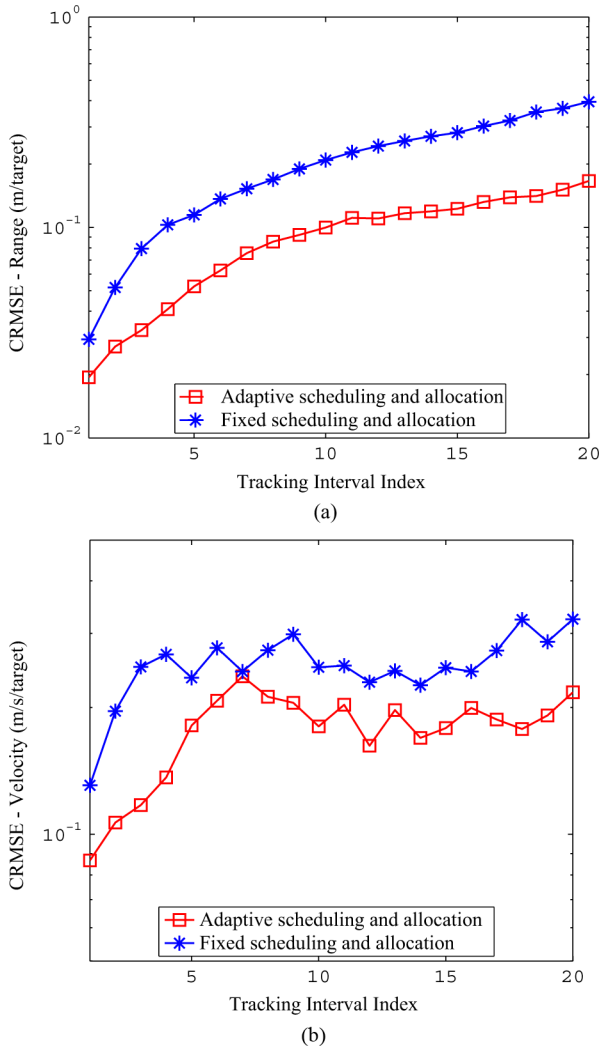
Fig. 4. Performance comparison with and without adaptive scheduling and power allocation for the second configuration. (a) CRMSE in range. (b) CRMSE in velocity.

TABLE III
TABLE SHOWING OUTPUT OF THE ANTENNA SCHEDULING FOR
ONE MONTE CARLO ITERATION

Tracking Inter- val Index	# of Antennas (second configuration)	Antennas selected (second configuration)	# of Antennas (third configuration)	Antennas selected (third configuration)
1	4	1,2,3,4	5	1,6,2,3,4
2	4	1,2,3,4	5	1,8,6,2,4
3	4	1,2,3,4	5	1,8,2,3,4
4	3	1,4,7	5	1,8,2,3,4
5	3	1,7,4	5	1,8,2,3,4
6	3	1,7,4	5	1,8,3,2,4
7	3	1,7,4	5	1,8,3,2,4
8	3	1,7,4	5	1,8,3,2,4
9	3	1,7,4	4	1,2,5,6
10	3	1,7,4	4	1,8,3,7
11	3	1,7,4	4	1,8,3,7
12	3	1,7,4	4	1,7,3,6
13	3	1,7,4	4	1,6,3,7
14	3	1,7,4	4	1,6,3,7
15	3	1,8,3	5	1,8,6,2,4
16	3	1,8,3	5	1,8,6,2,4
17	2	1,7	2	1,6
18	2	1,7	2	1,6
19	2	1,8	2	1,6
20	2	1,8	5	1,6,7,2,4

used the second configuration with $N_s = 200$ particles for this example. The parameter η_c was chosen to be 40. In Fig. 4, we plot the CMRSE in the range and the velocity estimates for this configuration. For the fixed scheduling and resource allocation, we used antennas $\{1, 2, 4\}$ and distributed the available power equally among them. We used three antennas so that the average number of antennas that are used remain same for both the adaptive case and the nonadaptive case. Using adaptive scheduling, four antennas were selected initially (see Table III). Since the RMSE is inversely proportional to the number of the antennas, maximum number of antennas were used within the distance constraint. As the target moved away from the fusion center, the antennas that are closer to the target are used, although this increased the communication cost. As a result only two antennas were selected after a few iterations. As it can be seen, the performance using adaptive scheduling and resource allocation was better compared to the performance obtained using the fixed scheduling resource allocation.

Example 3: In this example, we used third configuration with $N_s = 200$ particles and compared the performance of cognitive radar employing adaptive scheduling and resource allocation with the performance of the standard radar that employed fixed scheduling. The parameter η_c was chosen to be 120 for this example. In Fig. 5, we plot the CRMSE in the range and the velocity estimates of both the targets for this configuration. For the fixed scheduling, we used antenna set $\{1, 3, 7, 9\}$. As it can be seen the performance using adaptive scheduling and resource allocation was better compared to the performance obtained using the fixed scheduling resource allocation.

Example 4: In this example, we demonstrate the advantage of the multipath modeling in the system. In Fig. 6, we plot the CRMSE in the range and the velocity estimates obtained using

Example 1: In this example, we demonstrate the advantage of the proposed multiple Rao-Blackwellized particle filtering method. We considered the first configuration for this example. In Fig. 3, we plot the CRMSE averaged over all the 20 tracking intervals as a function of number of the particles for both SPF and the proposed MRBPF. It can be seen from the figure that MRBPF-based filtering resulted in lower CRMSE compared to the SPF-based filtering. This performance improvement is obtained since the MRBPF partitions the state space and computes the actual estimates of the channel state, and it updates the weight of individual target states instead of the joint target state. It can also be seen that we can achieve a given performance level using a MRBPF with fewer particles instead of a SPF with more particles. For example, to obtain an average CMRSE of 0.1 m/target we need approximately 80 particles using an MRBPF whereas we need around 160 particles using a SPF. Hence, MRBPF is computationally less expensive compared to the SPF, since we can get similar performance to that of SPF using fewer particles.

Example 2: In this example, we demonstrate the advantage of the adaptive scheduling and resource allocation methods. We
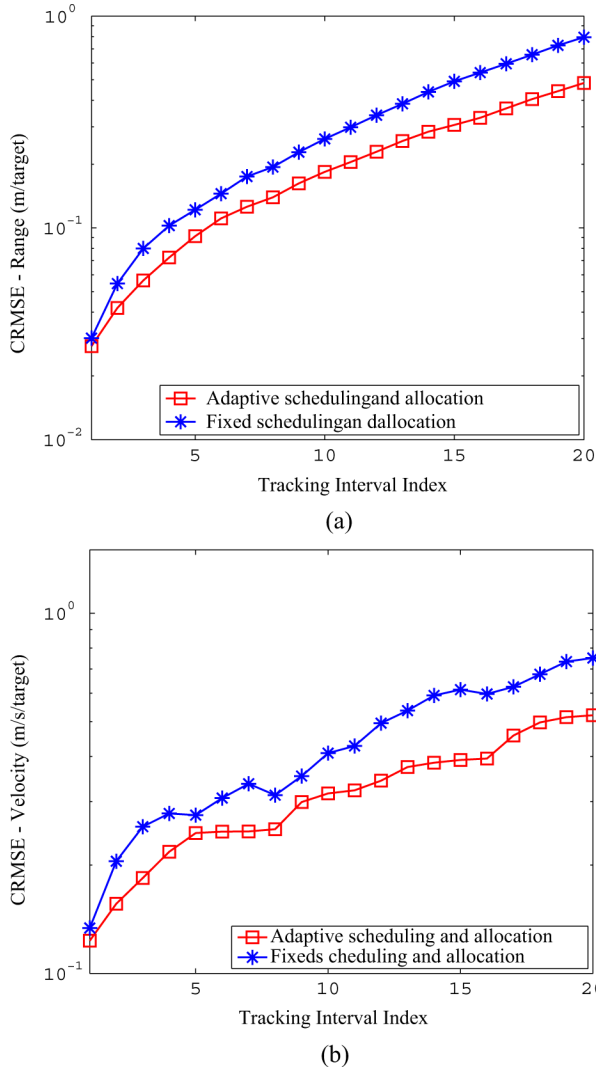
Fig. 5. Performance comparison with and without adaptive scheduling and power allocation for the third configuration. (a) CRMSE in range. (b) CRMSE in velocity.

Fig. 6. Performance comparison with and without multipath modeling. (a) CRMSE in range. (b) CRMSE in velocity.

the MRBPF tracking with and without considering the multipath modeling. We used first configuration for this example with $N_s = 200$ particles. It can be seen that when the multipath model was not considered the CRMSE increased. For the same parameters, the performance by considering the effect of time-varying multipath channel model was significantly better. This is due to the additional degrees of freedom that an urban environment provides in the form of delay and Doppler diversity. When the receiver has information about the propagation conditions, it can exploit the multipath nature of the urban environment to obtain a better performance.

VI. Summary

We considered the problem of multiple target tracking in an urban scenario which is characterized by multiple delay and Doppler shifts. We developed a measurement model by considering a finite dimensional representation of the time-varying impulse response function of the urban transmission channel. We employed a cognitive radar network that uses a Monte Carlo based filter as an approximate Bayesian filter at the receiver.
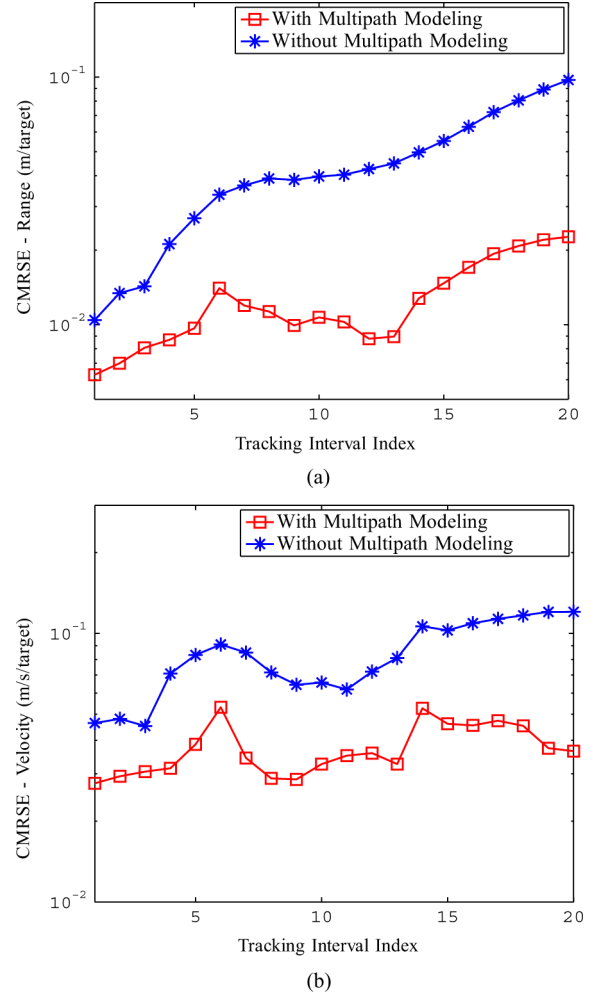
We proposed a new hybrid filter called the Multiple Rao-Blackwell particle filter (MRBPF) for the joint estimation of the target state and the channel state. The proposed filter was efficient for tracking high-dimensional state vector as it operates by partitioning the state space into lower dimensional subspaces. The global feedback enables the transmitter to choose an optimal subset of antennas and the power to be transmitted by each antenna. Since the optimal solution to the sensor scheduling and power allocation problem is NP-hard, we proposed a suboptimal, but computationally efficient, method for scheduling and power allocation based on greedy programming. We demonstrated through numerical simulations that the use of cognitive radar offers good performance compared to the standard radar, while reducing the communication costs. We also demonstrated the advantages of multipath modeling. In the future, we will develop waveform optimization techniques at the receiver based on the feedback from the transmitter. For a radar network with large number of antennas, computing the posterior Cramér-Rao bound (PCRB) will become cumbersome. We will develop other optimization criteria for such scenarios. We will also validate the accuracy of the proposed measurement model, performance of our proposed tracking filter, and the performance of the scheduling and resource allocation algorithms using real data.

APPENDIX
DERIVATION OF THE PCRB

Proof of Theorem 2: The log-likelihood of the measurement vector can be written as

$$\log p\left(\boldsymbol{y}_{k+1}|\boldsymbol{\xi}_{k+1}\right) = \log \prod_{p\in\pi_{k+1}} p\left(\boldsymbol{y}_{p,k+1}|\boldsymbol{\xi}_{k+1}\right)$$

$$= \sum_{p\in\pi_{k+1}} \left(\boldsymbol{y}_{p,k+1} - \boldsymbol{\mu}_{k+1}^p\right)^H$$

$$\times \boldsymbol{\Sigma}_{\mathrm{w},p}^{-1} \left(\boldsymbol{y}_{p,k+1} - \boldsymbol{\mu}_{k+1}^p\right) \qquad (46)$$

where

$$\boldsymbol{\mu}_{k+1}^p = \sum_{q\in\pi_{k+1}} \sum_{m\in\{1,\dots,M\}} \sqrt{\gamma_q \zeta_{pqm}} \boldsymbol{\Phi}_{pqm} \boldsymbol{\beta}_{pqm},$$

$$= \sum_{q\in\pi_{k+1}} \sqrt{\gamma_q} \boldsymbol{\mu}^{pq}. \qquad (47)$$

The Hessian of the log-likelihood with respect to the complex vector, $\boldsymbol{\xi}_{k+1}$, is evaluated as follows. See equation (48) at the bottom of the page. Therefore, we have

$$\mathbb{E}_{\boldsymbol{y}|\xi} \left[-\Delta_{\xi_{k+1}}^{\xi_{k+1}} \log p(\boldsymbol{y}_{k+1}|\boldsymbol{\xi}_{k+1}) \right]$$

$$= 2 \sum_{p\in\pi_{k+1}} \Re\left\{ \left(\frac{\partial\boldsymbol{\mu}_{k+1}^p}{\partial\boldsymbol{\xi}_{k+1}}\right) \boldsymbol{\Sigma}_{\mathrm{w},p}^{-1} \left(\frac{\partial\boldsymbol{\mu}_{k+1}^p}{\partial\boldsymbol{\xi}_{k+1}}\right)^H \right\}. \qquad (49)$$

Substituting the value of $\boldsymbol{\mu}_{k+1}^p$, we get

$$\mathbb{E}_{\boldsymbol{y}|\xi} \left[-\Delta_{\xi_{k+1}}^{\xi_{k+1}} \log p(\boldsymbol{y}_{k+1}|\boldsymbol{\xi}_{k+1}) \right]$$

$$= 2 \sum_{p,q,r\in\pi_{k+1}} \sqrt{\gamma_q \gamma_r} \Re\left\{ \left(\frac{\partial\boldsymbol{\mu}_{k+1}^{pq}}{\partial\boldsymbol{\xi}_{k+1}}\right) \boldsymbol{\Sigma}_{\mathrm{w},p}^{-1} \left(\frac{\partial\boldsymbol{\mu}_{k+1}^{pr}}{\partial\boldsymbol{\xi}_{k+1}}\right)^H \right\}. \qquad (50)$$

Evaluation of the Partial Derivatives: The partial derivative $\frac{\partial\boldsymbol{\mu}_{k+1}^{pq}}{\partial\boldsymbol{\xi}_{k+1}}$ can be computed as follows. First, the vector $\boldsymbol{\xi}_{k+1}$ is partitioned as $\boldsymbol{\xi}_{k+1} = \left[(\boldsymbol{\theta}_{k+1}^1)^T, \dots, (\boldsymbol{\theta}_{k+1}^M)^T, (\Re\{\boldsymbol{\beta}_{k+1}^{11}\})^T, (\Im\{\boldsymbol{\beta}_{k+1}^{11}\})^T, \dots, (\Re\{\boldsymbol{\beta}_{k+1}^{PP}\})^T, (\Im\{\boldsymbol{\beta}_{k+1}^{PP}\})^T\right]^T$. Following the definition of the complex vector differentiation [32], we have

$$\frac{\partial\boldsymbol{\mu}_{k+1}^{pq}}{\partial\boldsymbol{\xi}_{k+1}} = \left[\frac{\partial\boldsymbol{\mu}_{k+1}^{pq}}{\partial\boldsymbol{\theta}_{k+1}^1}, \dots, \frac{\partial\boldsymbol{\mu}_{k+1}^{pq}}{\partial\boldsymbol{\theta}_{k+1}^M}, \frac{\partial\boldsymbol{\mu}_{k+1}^{pq}}{\partial\boldsymbol{\beta}_{k+1}^{11}}, \dots, \frac{\partial\boldsymbol{\mu}_{k+1}^{pq}}{\partial\boldsymbol{\beta}_{k+1}^{PP}}\right],$$

$$= \left[\frac{\partial\boldsymbol{\mu}_{k+1}^{pq}}{\partial\boldsymbol{\theta}_{k+1}}, \frac{1}{2}\left(\frac{\partial\boldsymbol{\mu}_{k+1}^{pq}}{\partial\Re\{\boldsymbol{\beta}_{k+1}^{11}\}} - j\frac{\partial\boldsymbol{\mu}_{k+1}^{pq}}{\partial\Im\{\boldsymbol{\beta}_{k+1}^{11}\}}\right), \dots,\right.$$

$$\left.\frac{1}{2}\left(\frac{\partial\boldsymbol{\mu}_{k+1}^{pq}}{\partial\Re\{\boldsymbol{\beta}_{k+1}^{PP}\}} - j\frac{\partial\boldsymbol{\mu}_{k+1}^{pq}}{\partial\Im\{\boldsymbol{\beta}_{k+1}^{PP}\}}\right)\right] \qquad (51)$$

where the partial derivatives with respect to the target state and the channel state vector can be derived as follows:

- $\frac{\partial\boldsymbol{\mu}_{k+1}^{pq}}{\partial\boldsymbol{\theta}_{k+1}^m} = \sqrt{\zeta_{pqm}}\left(\boldsymbol{\beta}_{pqm}^T\otimes\boldsymbol{I}_{LN}\right)\frac{\partial\mathrm{vec}(\boldsymbol{\Phi}_{pqm})}{\partial\boldsymbol{\varphi}_{k+1}^{pqm}}\boldsymbol{\Lambda}^{pqm} + \frac{1}{2\sqrt{\zeta_{pqm}}}\boldsymbol{\Phi}_{pqm}\boldsymbol{\beta}_{pqm}\tilde{\boldsymbol{\Lambda}}^{pqm}$;

- $\boldsymbol{\varphi}^{pqm} = [\tau_{pqm}, \nu_{pqm}]^T$ is a vector of the delay-Dopplers corresponding to the mth target and the $q^{\mathrm{th}}, p^{\mathrm{th}}$ transmit-receive pair;

- $\boldsymbol{\Lambda}^{pqm} = \frac{\partial\boldsymbol{\varphi}^{pqm}}{\partial\boldsymbol{\theta}_{k+1}^m}$ is a 2×4 matrix;

- $\tilde{\boldsymbol{\Lambda}}^{pqm} = \frac{\partial\zeta_{pqm}}{\partial\boldsymbol{\theta}_{k+1}^m}$ is a 1×4 row vector;

- $\frac{\partial\boldsymbol{\mu}_{k+1}^{pq}}{\partial\Re\{\boldsymbol{\beta}_{k+1}^{uv}\}} = \frac{\partial\boldsymbol{\mu}_{k+1}^{pq}}{\partial\Im\{\boldsymbol{\beta}_{k+1}^{uv}\}} = \sqrt{\zeta_{pqm}}\delta(p-u)\delta(q-v)\boldsymbol{\Phi}_{pqm}$.

Here, the matrices $\boldsymbol{\Lambda}^{pqm}$, and $\tilde{\boldsymbol{\Lambda}}^{pqm}$ are given as

$$\boldsymbol{\Lambda}^{pqm} = \begin{bmatrix} \lambda_{11}^{pqm} & \lambda_{12}^{pqm} & \lambda_{13}^{pqm} & \lambda_{14}^{pqm} \\ \lambda_{21}^{pqm} & \lambda_{22}^{pqm} & \lambda_{23}^{pqm} & \lambda_{24}^{pqm} \end{bmatrix}$$

and

$$\tilde{\boldsymbol{\Lambda}}^{pqm} = \begin{bmatrix} \tilde{\lambda}_1^{pqm}, & \tilde{\lambda}_2^{pqm}, & \tilde{\lambda}_3^{pqm}, & \tilde{\lambda}_4^{pqm} \end{bmatrix}.$$

$$-\Delta_{\xi_{k+1}}^{\xi_{k+1}} \log p(\boldsymbol{y}_{k+1}|\boldsymbol{\xi}_{k+1})$$

$$= -\Delta_{\xi_{k+1}}\left\{\Delta_{\xi_{k+1}} \log p(\boldsymbol{y}_{k+1}|\boldsymbol{\xi}_{k+1})\right\}^H$$

$$= -\sum_{p\in\pi_{k+1}} \Delta_{\xi_{k+1}}\left\{\Delta_{\xi_{k+1}}(\boldsymbol{y}_{p,k+1} - \boldsymbol{\mu}_{k+1}^p)^H\boldsymbol{\Sigma}_{\mathrm{w},p}^{-1}(\boldsymbol{y}_{p,k+1} - \boldsymbol{\mu}_{k+1}^p)\right\}^H$$

$$= -\sum_{p\in\pi_{k+1}} \Delta_{\xi_{k+1}}\left\{\left(\frac{\partial\boldsymbol{\mu}_{k+1}^p}{\partial\boldsymbol{\xi}_{k+1}}\right)\frac{\partial}{\partial\boldsymbol{\mu}_{k+1}^p}(\boldsymbol{y}_{p,k+1} - \boldsymbol{\mu}_{k+1}^p)^H\boldsymbol{\Sigma}_{\mathrm{w},p}^{-1}(\boldsymbol{y}_{p,k+1} - \boldsymbol{\mu}_{k+1}^p)\right\}^H$$

$$= -2\sum_{p\in\pi_{k+1}} \Re\left\{\Delta_{\xi_{k+1}}\boldsymbol{\Sigma}_{\mathrm{w},p}^{-1}\left(\boldsymbol{y}_{p,k+1} - \boldsymbol{\mu}_{k+1}^p\right)\left(\frac{\partial\boldsymbol{\mu}_{k+1}^p}{\partial\boldsymbol{\xi}_{k+1}}\right)^H\right\}$$

$$= -2\sum_{p\in\pi_{k+1}} \Re\left\{\boldsymbol{\Sigma}_{\mathrm{w},p}^{-1}\left(\boldsymbol{y}_{p,k+1} - \boldsymbol{\mu}_{k+1}^p\right)\frac{\partial}{\partial\boldsymbol{\xi}_{k+1}}\left(\frac{\partial\boldsymbol{\mu}_{k+1}^p}{\partial\boldsymbol{\xi}_{k+1}}\right)^H - \left(\frac{\partial\boldsymbol{\mu}_{k+1}^p}{\partial\boldsymbol{\xi}_{k+1}}\right)\boldsymbol{\Sigma}_{\mathrm{w},p}^{-1}\left(\frac{\partial\boldsymbol{\mu}_{k+1}^p}{\partial\boldsymbol{\xi}_{k+1}}\right)^H\right\}. \qquad (48)$$

The elements of $\mathbf{\Lambda}^{pqm}$ are given as [33]

$$\lambda_{11}^{pqm} = \frac{\partial \tau_{pqm}}{\partial x_m} = \frac{1}{c}\left(\frac{x_q - x_m}{R_{qm}} + \frac{x_p - x_m}{R_{pm}}\right)$$

$$\lambda_{12}^{pqm} = \frac{\partial \tau_{pqm}}{\partial y_m} = \frac{1}{c}\left(\frac{y_q - y_m}{R_{qm}} + \frac{y_p - y_m}{R_{pm}}\right)$$

$$\lambda_{13}^{pqm} = \frac{\partial \tau_{pqm}}{\partial \dot{x}_m} = 0$$

$$\lambda_{14}^{pqm} = \frac{\partial \tau_{pqm}}{\partial \dot{y}_m} = 0$$

$$\lambda_{21}^{pqm} = \frac{\partial \nu_{pqm}}{\partial x_m} = \frac{f_c}{c}\left(\frac{\dot{x}_m}{R_{qm}} - \dot{R}_{qm}\frac{x_q - x_m}{R_{qm}^2}\right.$$
$$\left. + \frac{\dot{x}_m}{R_{pm}} - \dot{R}_{pm}\frac{x_p - x_m}{R_{pm}^2}\right)$$

$$\lambda_{22}^{pqm} = \frac{\partial \nu_{pqm}}{\partial y_m} = \frac{f_c}{c}\left(\frac{\dot{y}_m}{R_{qm}} - \dot{R}_{qm}\frac{y_q - y_m}{R_{qm}^2}\right.$$
$$\left. + \frac{\dot{y}_m}{R_{pm}} - \dot{R}_{pm}\frac{y_p - y_m}{R_{pm}^2}\right)$$

$$\lambda_{23}^{pqm} = \frac{\partial \nu_{pqm}}{\partial \dot{x}_m} = \frac{f_c}{c}\left(\frac{x_q - x_m}{R_{qm}} + \frac{x_p - x_m}{R_{pm}}\right)$$

$$\lambda_{24}^{pqm} = \frac{\partial \nu_{pqm}}{\partial \dot{y}_m} = \frac{f_c}{c}\left(\frac{y_q - y_m}{R_{qm}} + \frac{y_p - y_m}{R_{pm}}\right) \qquad (52)$$

and the elements of $\tilde{\mathbf{\Lambda}}^{pqm}$ are given as

$$\tilde{\lambda}_1^{pqm} = \frac{\partial \zeta_{pqm}}{\partial x_m} = \zeta_{pqm}\left(\frac{x_q - x_m}{R_{qm}^2} + \frac{x_p - x_m}{R_{pm}^2}\right)$$

$$\tilde{\lambda}_2^{pqm} = \frac{\partial \zeta_{pqm}}{\partial y_m} = \zeta_{pqm}\left(\frac{y_q - y_m}{R_{qm}^2} + \frac{y_p - y_m}{R_{pm}^2}\right)$$

$$\tilde{\lambda}_3^{pqm} = \frac{\partial \zeta_{pqm}}{\partial \dot{x}_m} = 0$$

$$\tilde{\lambda}_4^{pqm} = \frac{\partial \zeta_{pqm}}{\partial \dot{y}_m} = 0.$$

REFERENCES

[1] S. Haykin, "Cognitive radar: A way of the future," *IEEE Signal Process. Mag.*, vol. 23, no. 1, pp. 30–40, 2006.

[2] S. Haykin, "Cognitive radar networks," in *Proc. 4th IEEE Workshop Sensor Array Multichannel Process.*, Boston, MA, Jul. 2006, pp. 1–24.

[3] N. A. Goodman, P. R. Venkata, and M. A. Neifeld, "Adaptive waveform design and sequential hypothesis testing for target recognition with active sensors," *IEEE J. Sel. Topics Signal Process.*, vol. 1, no. 1, pp. 105–113, 2007.

[4] Y. Nijsure, Y. Chen, P. Rapajic, C. Yuen, Y. H. Chew, and T. F. Qin, "Information-theoretic algorithm for waveform optimization within ultra wideband cognitive radar network," in *Proc. EEE Int. Conf. Ultra-Wideband*, Sep. 2010, vol. 2, pp. 1–4.

[5] P. Chavali and A. Nehorai, "Cognitive radar for target tracking in multipath scenarios," in *Proc. Int. Waveform Diversity Des. (WDD) Conf.*, Niagara Falls, Canada, Aug. 2010, pp. 110–114.

[6] S. Haykin, A. Zia, I. Arasaratnam, and X. Yanbo, "Cognitive tracking radar," in *Proc. Radar Conf.*, Washington, DC, May 10–14, 2010, pp. 1467–1470.

[7] Y. Wei, H. Meng, Y. Liu, and X. Wang, "Extended target recognition in cognitive radar networks," *Sensors*, vol. 10, no. 11, pp. 10 181–10 197, 2010.

[8] Y. Wei, H. Meng, and X. Wang, "Adaptive single-tone waveform design for target recognition in cognitive radar," in *Proc. IET Int. Radar Conf.*, Guilin, China, Apr. 2009, vol. 2009, pp. 707–711.

[9] L. Fan, J. Wang, B. Wang, and D. Shu, "Time resources allocation in cognitive radar system," in *Proc. Int. Conf. Netw., Sens., Control*, Chicago, IL, Apr. 2010, pp. 727–730.

[10] S. Blackman and R. Popoli, *Design and Analysis of Modern Tracking Systems*. Noorwood, MA: Artech House, 1999, vol. 685.

[11] J. L. Krolik, J. Farrell, and A. Steinhardt, "Exploiting multipath propagation for GMTI in urban environments," in *Proc. Radar Conf.*, Verona, NY, Apr. 24–27, 2006, pp. 65–68.

[12] B. Chakraborty, Y. Li, J. J. Zhang, T. Trueblood, A. Papandreou-Suppappola, and D. Morrell, "Multipath exploitation with adaptive waveform design for target tracking in urban terrain," in *Proc. Int. Conf. Acoust., Speech, Signal Process.*, Dallas, TX, Mar. 14–19, 2010, pp. 3894–3897.

[13] Y. Jin, J. M. Moura, and N. O'Donoughue, "Time reversal in multiple-input multiple-output radar," *IEEE J. Sel. Topics Signal Process.*, vol. 4, no. 1, pp. 210–225, Feb. 2010.

[14] M. Hurtado, T. Zhao, and A. Nehorai, "Adaptive polarized waveform design for target tracking based on sequential Bayesian inference," *IEEE Trans. Signal Process.*, vol. 56, pp. 1120–1133, Mar. 2008.

[15] S. Joshi and S. Boyd, "Sensor selection via convex optimization," *IEEE Trans. Signal Process.*, vol. 57, no. 2, pp. 451–462, Feb. 2009.

[16] H. Godrich, A. Petropulu, and H. V. Poor, "Resource allocation schemes for target localization in distributed multiple radar architectures," presented at the Eur. Signal Process. Conf., Aalborg, Denmark, Aug. 23–27, 2010.

[17] H. Godrich, A. Petropulu, and H. V. Poor, "A combinatorial optimization framework for subset selection in distributed multiple-radar architectures," presented at the Int. Conf. Acoust., Speech, Signal Process., Prague, Czech Republic, May 2011.

[18] R. Tharmarasa, T. Kirubarajan, M. L. Hernandez, and A. Sinha, "PCRLB-based multisensor array management for multitarget tracking," *IEEE Trans. Aerosp. Electron. Syst.*, vol. 43, no. 2, pp. 539–555, Apr. 2007.

[19] P. Chavali and A. Nehorai, "A low-complexity sparsity-based multi-target tracking algorithm for urban environments," presented at the Proc. Radar Conf., Kansas City, May 23–27, 2011.

[20] A. Pandharipande, "Principles of OFDM," *IEEE Potentials*, vol. 21, no. 2, pp. 16–19, Apr. 2002.

[21] Y. Bar-Shalom, X.-R Li, and T. Kirubarajan, *Estimation with Applications to Tracking and Navigation*. New York: Wiley, 2001.

[22] S. M. Kay, *Fundamentals of Statistical Signal Processing, Estimation Theory*. Englewood Cliffs, NJ: Prentice-Hall, 1993, vol. 1.

[23] M. S. Arulampalam, S. Maskell, N. J. Gordon, and T. Clapp, "A tutorial on particle filters for online nonlinear/non-Gaussian Bayesian tracking," *IEEE Trans. Signal Process.*, vol. 50, no. 2, pp. 174–188, Feb. 2002.

[24] B. Ristic, S. Arulampalam, and S. Gordon, *Beyond the Kalman Filter: Particle Filters for Tracking Applications*. Norwood, MA: Artech House, 2004.

[25] A. Doucet, "On sequential Monte Carlo methods for Bayesian filtering," Dept. of Eng., Univ. of Cambridge, Cambridge, U.K., 1998.

[26] N. J. Gordon, D. J. Salmond, and A. F. M. Smith, "Novel approach to nonlinear/non-Gaussian Bayesian state estimation," *Proc. IEEE Radar Signal Process.*, vol. 140, no. 2, pp. 107–113, Apr. 1993.

[27] M. F. Bugallo, L. Ting, and P. M. Djuric, "Target tracking by multiple particle filtering," in *Proc. Aerospace Conf.*, Big Sky, MT, Mar. 2007, pp. 1–7.

[28] T. Schon, G. Gustafsson, and P. J. Nordlund, "Marginalized particle filters for mixed linear/nonlinear state-space models," *IEEE Trans. Signal Process.*, vol. 53, no. 7, pp. 2279–2289, Jul. 2005.

[29] M. Frederic, M. Bolic, and M. Bouchard, "Rao-Blackwellised particle filters: Examples of applications," in *Proc. Can. Conf. Electr. Comput. Eng.*, Ottawa, ON, Canada, May 2006, pp. 1196–1200.

[30] A. Doucet, N. De Freitas, K. Murphy, and S. Russell, "Rao-Blackwellised particle filtering for dynamic Bayesian networks," in *Proc. 16th Conf. Uncertainty Art. Intell.*, Citeseer, 2000, pp. 176–183.

[31] P. Tichavský, C. H. Muravchik, and A. Nehorai, "Posterior Cramér-Rao bounds for discrete-time nonlinear filtering," *IEEE Trans. Signal Process.*, vol. 46, no. 5, May 1998.

[32] A. Hjorungnes and D. Gesbert, "Complex-valued matrix differentiation: Techniques and key results," *IEEE Trans. Signal Process.*, vol. 55, no. 6, pp. 2740–2746, Jun. 2007.

[33] J. Zhang, B. Manjunath, A. Papandreou-Suppappola, and D. Morell, "Dynamic waveform design for target tracking using MIMO radar," in *Proc. Asilomar Conf. Signals, Syst., Comput.*, Asilomar, CA, Oct. 2008, pp. 31–35.

Phani Chavali (S'08) received the B.Tech. degree in electronics and communications engineering (with Honors in signal processing and communications) from the International Institute of Information Technology-Hyderabad, India, in 2007 and the M.S. degree in electrical engineering from Washington University in St. Louis (WUSTL) in 2010. He is currently working towards the Ph.D. degree in the electrical and systems engineering from WUSTL.

Prior to joining WUSTL, he was employed with the Wireless Terminal Division of Samsung Electronics in Bangalore, India. His research interests are broadly in the areas of statistical signal processing, radar systems, optimization techniques, Monte Carlo methods, learning and inference algorithms.

Arye Nehorai (S'80–M'83–SM'90–F'94) received the B.Sc. and M.Sc. degrees from the Technion—Israel Institute of Technology, Haifa, and the Ph.D. from Stanford University, Stanford, CA.

He was formerly a faculty member at Yale University and the University of Illinois at Chicago. He is currently the Eugene and Martha Lohman Professor and Chair of The Preston M. Green Department of Electrical and Systems Engineering at Washington University in St. Louis (WUSTL). He serves as the Director of the Center for Sensor Signal and Information Processing at WUSTL.

Dr. Nehorai served as Editor-in-Chief of the IEEE TRANSACTIONS ON SIGNAL PROCESSING from 2000 to 2002. From 2003 to 2005, he was Vice-President (Publications) of the IEEE Signal Processing Society (SPS), Chair of the Publications Board, and member of the Executive Committee of this Society. He was the Founding Editor of the special columns on Leadership Reflections in the IEEE SIGNAL PROCESSING MAGAZINE from 2003 to 2006. He received the 2006 IEEE SPS Technical Achievement Award and the 2010 IEEE SPS Meritorious Service Award. He was elected Distinguished Lecturer of the IEEE SPS for the term 2004 to 2005. He was corecipient of the IEEE SPS 1989 Senior Award for Best Paper coauthor of the 2003 Young Author Best Paper Award and corecipient of the 2004 Magazine Paper Award. In 2001, he was named University Scholar of the University of Illinois. He has been a Fellow of the Royal Statistical Society since 1996.